nature communications

Article

https://doi.org/10.1038/s41467-025-58212-8

A Csde1-Strap complex regulates plasma cell differentiation by coupling mRNA translation and decay

Received: 2 March 2024

Accepted: 13 March 2025

Published online: 25 March 2025

Check for updates

Pengda Chen[1,8], Lianghua Lin[1,8], Xinyong Lin[1,8], Kunyu Liao[1,8], Jiali Qiang[2,8], Zhizhang Wang[3], Jianfeng Wu[1], Yang Li[4], Liang Yang[5], Nan Yao[5], Huilin Song[1], Yazhen Hong[1], Wen-Hsien Liu[1] ✉, Yaoyang Zhang[2] ✉, Xing Chang[3] ✉, Dan Du[6] ✉ & Changchun Xiao[1,7] ✉

Upon encountering antigens, B cells may undergo multiple differentiation paths, including becoming plasma cells and memory B cells. Although it is well-known that transcription factors govern gene expression programs underpinning these fate decisions in transcriptional level, the role of post-transcriptional regulators, with a focus on RNA-binding proteins, in the fate determination are lesser known. Here we find by RNA interactome capture-coupled CRISPR/Cas9 functional screening that the Csde1-Strap complex plays an important role in plasma cell differentiation. Mechanistically, the Csde1-Strap complex establishes the expression kinetics of Bach2, a key regulator of plasma cell differentiation. Bach2 expression is rapidly induced to promote B cell expansion and then decreased to initiate plasma cell differentiation. The Csde1-Strap interaction is critical for their binding to *Bach2* mRNA to couple its decay with translation to restrain the magnitude and duration of Bach2 protein expression. In the absence of Csde1 or Strap, Bach2 translation is de-coupled from mRNA decay, leading to elevated and prolonged expression of Bach2 protein and impaired plasma cell differentiation. This study thus establishes the functional RBP landscape in B cells and illustrates the fundamental importance of controlling protein expression kinetics in cell fate determination.

Cells often undergo rapid activation, proliferation, and differentiation in response to environmental signals. Exquisite control of protein expression kinetics is pivotal for orchestrating these highly dynamic processes, as cells need to make the right proteins in the right amounts, in the right place, and at the right time to function properly. Transcription, epigenetic regulation, and protein degradation have been shown to play critical roles in achieving precise control of protein expression[1–5]. In contrast, the

[1]State Key Laboratory of Cellular Stress Biology, School of Life Sciences, Faculty of Medicine and Life Sciences, Xiamen University, Xiamen, Fujian, China. [2]Interdisciplinary Research Center on Biology and Chemistry, Shanghai Institute of Organic Chemistry, Chinese Academy of Sciences, Shanghai, China. [3]Hangzhou First People's Hospital, School of Medicine, Westlake University, Hangzhou, China. [4]CAS Key Laboratory of Tissue Microenvironment and Tumor, Shanghai Institute of Nutrition and Health, University of Chinese Academy of Sciences, Chinese Academy of Sciences, Shanghai, China. [5]Westlake Laboratory of Life Sciences and Biomedicine, Key Laboratory of Structural Biology of Zhejiang Province, School of Life Sciences, Westlake University, Hangzhou, Zhejiang Province, China. [6]State Key Laboratory of Cellular Stress Biology, Department of Gastroenterology, Zhongshan Hospital of Xiamen University, School of Medicine, Faculty of Medicine and Life Sciences, Xiamen University, Xiamen, Fujian, China. [7]Department of Immunology and Microbiology, The Scripps Research Institute, La Jolla, CA, USA. [8]These authors contributed equally: Pengda Chen, Lianghua Lin, Xinyong Lin, Kunyu Liao, Jiali Qiang.
✉e-mail: whliu@xmu.edu.cn; zyy@sioc.ac.cn; changxing@westlake.edu.cn; dandu@xmu.edu.cn; cxiao@scripps.edu

roles of mRNA translation and decay in this process remain poorly understood.

A growing body of evidence suggests that a large portion of mRNA decay mediated by deadenylation occurs co-translationally[6]. Co-translational decay is essential for mRNA quality control through nonsense-mediated decay (NMD). Moreover, major coding-region determinant (mCRD)-mediated mRNA decay, which regulates mRNA deadenylation when ribosomes transit through the coding sequence, is essential for the transient upregulation of primary response genes such as *c-Myc* and *c-Fos*[7]. Previous studies have shown that cis-elements in 5′ and 3′ untranslated regions (UTRs), as well as those located in the coding sequence (CDS) region, work together to regulate translation and decay of mRNA transcripts[8,9]. However, the identity of those cis-elements, the associated RNA-binding proteins (RBPs) and microRNAs (miRNAs), their biological functions and underlying regulatory mechanisms are yet to be unraveled.

We aim to identify the key players and mechanisms of actions regulating mRNA translation and decay in the mammalian immune system. B cells are particularly suitable for this purpose. As the antibody-producing cells of our body, B cells undergo many rounds of activation, proliferation, and fate determination in their life cycle. Naïve B cells reside in B cell follicles of secondary lymphoid tissues such as the spleen and lymph nodes. They are quiescent and do not secrete antibodies. Upon exposure to appropriate stimuli, B cells grow in size, start to proliferate, and migrate to the border of B cell follicles to interact with T cells. Activated B cells can either form extrafollicular foci or enter a specialized structure called germinal center (GC), where they interact with a distinct subset of $CD4^+$ effector T cells named T follicular helper (T_{FH}) cells. Upon stimulation by CD40L and cytokines such as IL-21 from T_{FH} cells[10], GC B (GCB) cells undergo extensive proliferation, class-switch recombination, somatic hypermutation, and differentiation into plasma cells and memory B cells. This T-dependent B cell response ultimately leads to generation of long-lived plasma cells sustaining antibody production and memory B cells that maintain the B cell phenotype but are programmed to rapidly differentiate into plasma cells upon encountering the same antigen.

The current model of plasma cell differentiation is a model of mutual antagonism between two sets of transcription factors: those that govern mature B and GCB cells, such as Pax5, Bcl6, Bach2, and Mitf, versus those that dictate the plasma cell program, such as Irf4, Blimp1, and Xbp1. Central to this model is the ability of those two sets of transcription factors to repress each other's expression, such that the latter must gain functional dominance against the former for plasma cell differentiation to occur. Some of those key transcription factors, such as Irf4 and Bach2, exert pleiotropic effects on cell fate determination through dynamic expression[11–13]. While the transcriptional networks and signaling pathways connecting them with environmental cues to control plasma cell differentiation have been extensively studied in the past decades, recent studies suggest that RBPs and miRNAs also play critical roles in this process[13–17].

In this study, we employ RNA-interactome capture (RIC) technology to identify RNA-binding proteins (RBP) in an in vitro model of plasma cell differentiation. Using CRISPR/Cas9-mediated screening, we assess their functions and discover a Csde1-Strap complex that plays a crucial role in T cell-dependent immune responses. Further molecular analyses identify key target genes of Csde1 and Strap, revealing that coupling mRNA translation and decay is a major mechanism regulating Bach2 protein expression kinetics. Collectively, this study identifies essential RBPs regulating plasma cell differentiation and highlights a tightly associated RBP complex that regulates the protein expression kinetics of a key transcription factor controlling B cell differentiation. These findings underscore the fundamental role of post-transcriptional regulation in cell fate determination and the critical importance of precise control of protein expression kinetics in coordinating dynamic cellular processes.

Results

Identification of differentiation stage-specific RBPomes via mRNA-interactome capture

We performed mRNA interactome capture (RIC) to identify RBPs expressed at different stages of plasma cell differentiation in an in vitro culture system mimicking B cell differentiation into plasma cells[18]. In this system, naive mouse B cells were cultured on top of Balb/c 3T3 cells stably expressing CD40L and Baff (termed 40LB cells)[19]. In the presence of IL-4, naïve B cells acquire a germinal center B (GCB) cell phenotype ($Fas^+GL\text{-}7^+Bcl6^+$, termed iGCB cells) after 4 days of culture. Those iGCB cells can further differentiate into plasma cells (termed iPC cells) after 4 additional days of culture on 40LB cells in the presence of IL-21 (Fig. 1a). After UV crosslinking of naïve B, iGCB, and iPC cells, poly(A) RNA was precipitated by oligo (dT) beads, treated with RNase to remove RNA, and RNA-associated proteins were analyzed by mass spectrometry (Fig. 1a). As shown in Supplementary Fig. 1a, silver staining revealed a protein pool bound to poly(A) RNA and demonstrated UV crosslinking-dependency of RNA interactome capture (RIC). Immunoblotting and qRT-PCR analyses showed that known RBPs and poly(A) RNA were precipitated by oligo (dT) beads, but not RNAs with no poly(A) and non-RBP proteins (Supplementary Fig. 1b, c). The RIC experiments were repeated multiple times in naïve B, iGCB, and iPC cells, with good reproducibility (Supplementary Fig. 1d, e). A total of 175, 457, and 556 proteins were identified in naïve B, iGCB, and iPC cells, respectively (Fig. 1b and Supplementary Data 1). The RBP composition of naïve B, iGCB, and iPC cells largely resemble RBPomes previously identified in mESC[20], MEF[21], Raw264.7[22], and HL.1[23], with some B cell-specific ones (Supplementary Fig. 2a, b). Among RBPs identified in naïve B, iGCB, and iPC cells, those annotated by the Gene Ontology term "RNA-binding" were classified as canonical RBPs. Most of them contain known RNA-binding domains (RBDs) in eukaryotic cells. Among non-canonical RBPs identified in naïve B, iGCB, and iPC cells, 10, 35, and 62 were not previously identified as RNA binding proteins in EuRBPDB[24] database and are therefore categorized as new RBPs (Fig. 1c and Supplementary Data 2). Interestingly, iGCB and iPC cells shared most canonical RBPs (246) but only a small portion of non-canonical RBPs (Fig. 1d). The number of RBPs identified in naïve B cells was much less than iGCB and iPC cells. While canonical RBPs in naïve B cells largely overlapped with those in iGCB and iPC cells, non-canonical RBPs were quite different among those three types of cells (Fig. 1d). These results suggest the existence of a group of core RBPs performing functions common to all cell types, as well as other RBPs performing cell type-specific functions.

We performed Gene Ontology (GO) analysis of these RBPs to gain insights into their biological functions. Canonical RBPs identified in iGCB and iPC cells harbored a number of common functional clusters, including "mRNA metabolic process", "ribonucleoprotein complex biogenesis"[25], "translation"[26] and "spliceosomal complex"[27,28], while non-canonical RBPs in iGCB and iPC cells contained different functional clusters, which may associate with cell type-specific functions (Supplementary Fig. 2c-e). Importantly, translation is among the most enriched biological processes associated with canonical RBPs identified in iGCB and iPC cells, as well as non-canonical RBPs identified in iGCB, suggesting a central role of translational control during plasma cell differentiation (Supplementary Fig. 2c-e). Notably, GO analysis performed with canonical RBPs in naïve B cells shared with iGCB and iPC cells enrichment of functional clusters of "mRNA metabolism" and "RNA splicing", but not translation. Instead, "stress granule assembly" is enriched in naïve B cells. Together, those results reflect the quiescence of naive B cells, in which translationally inactive mRNAs are enriched in stress granules[29], and suggest critical roles of translation during B cell activation (Supplementary Fig. 2c)[30].

Functional analysis of RBPs during plasma cell differentiation

We next employed CRISPR/Cas9-mediated functional screening to evaluate the biological roles of RBPs during plasma cell

https://doi.org/10.1038/s41467-025-58212-8

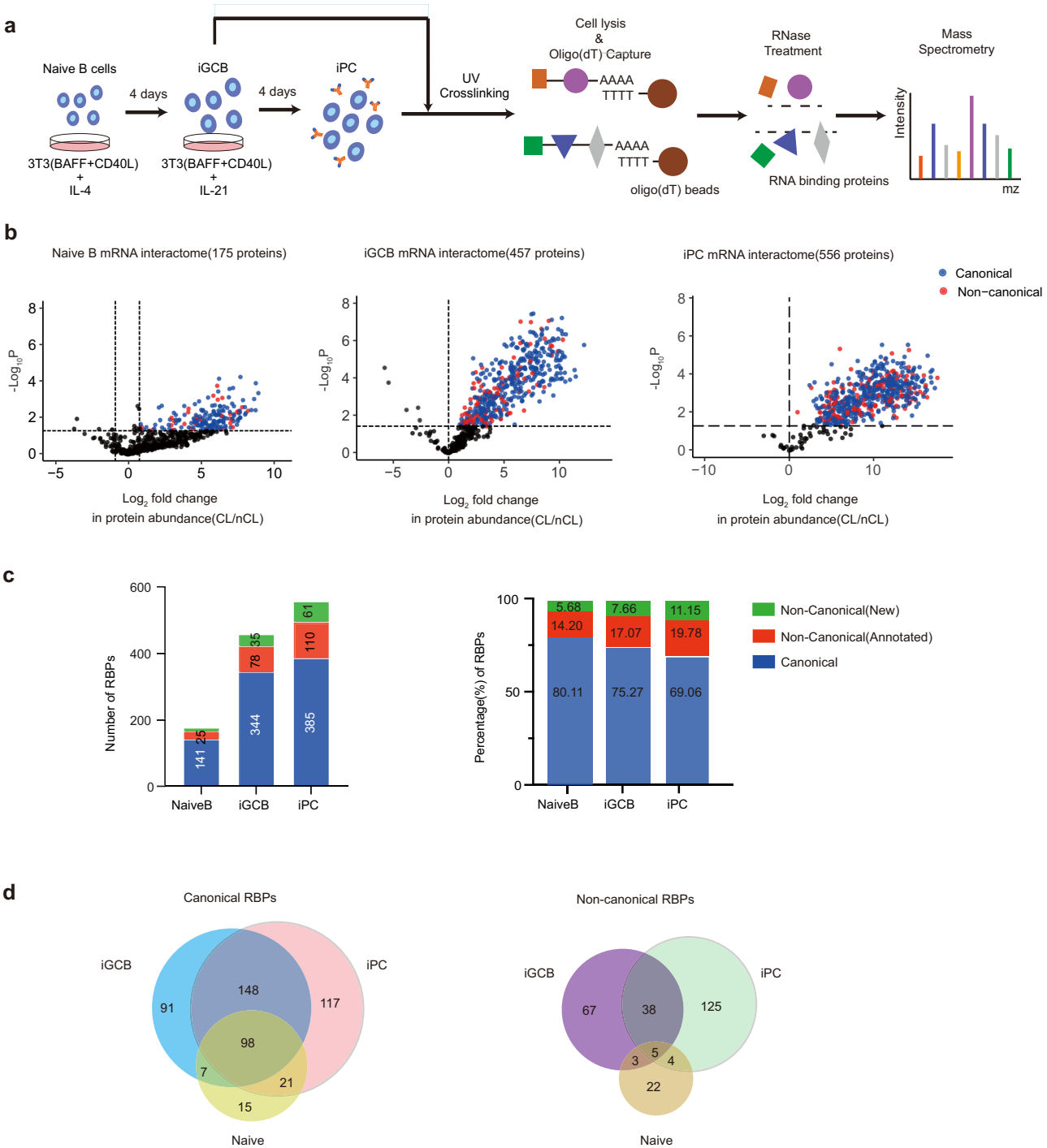

Fig. 1 | Identification of RBPs during plasma cell differentiation via mRNA-interactome capture. a Workflow for mRNA interactome capture. **b** The volcano plots summarizing proteins pulled down by poly(A) RNA. CL, UV-crosslinked; nCL, without UV crosslinking. Blue dots indicate canonical RBPs while red dots indicate non-canonical RBPs of the RBPomes. Statistical analyses were performed using two-tailed one sample Student's t-test for the change of protein abundance in cross-linking and non-crosslinking groups. **c** Bar graphs showing the numbers and percentages of canonical, non-canonical (annotated), and non-canonical (new) RBPs identified in naïve B, iGCB and iPC cells. **d** Venn diagrams summarizing the overlap of canonical and non-canonical RBPs identified in naïve B, iGCB, and iPC cells.

differentiation[31]. We first tested the screening condition by mixing naïve B cells from *Rosa26-Cas9-GFP* (CD45.2$^+$) and wild type (CD45.1$^+$) mice in a 1:1 ratio, and culturing cells in the in vitro plasma cell differentiation system (Fig. 2a). Consistent with previous reports[32,33], sgRNA targeting Myc mainly reduced the number of Cas9$^+$ cells, while sgRNA targeting Prdm1 significantly impaired plasma cell differentiation (Supplementary Fig. 3a). The successful editing of Myc and Prdm1 genes was confirmed by sequencing (Supplementary Fig. 3f). We compiled a list of 759 mouse RBP genes including all RBPs identified in iGCB and iPC cells and generated a retroviral library encoding sgRNAs targeting those genes (Supplementary Fig. 3b and Supplementary Data 3). This library encodes 4 - 8 sgRNAs per RBP gene, as well as sgRNAs targeting 9 positive control genes and 350 non-targeting control (NTC) sgRNAs. In total, this library contains 4039 sgRNAs with more than 80% of them distributed within a 2.9-fold range (Supplementary Fig. 3c-e; Supplementary Data 4).

https://doi.org/10.1038/s41467-025-58212-8

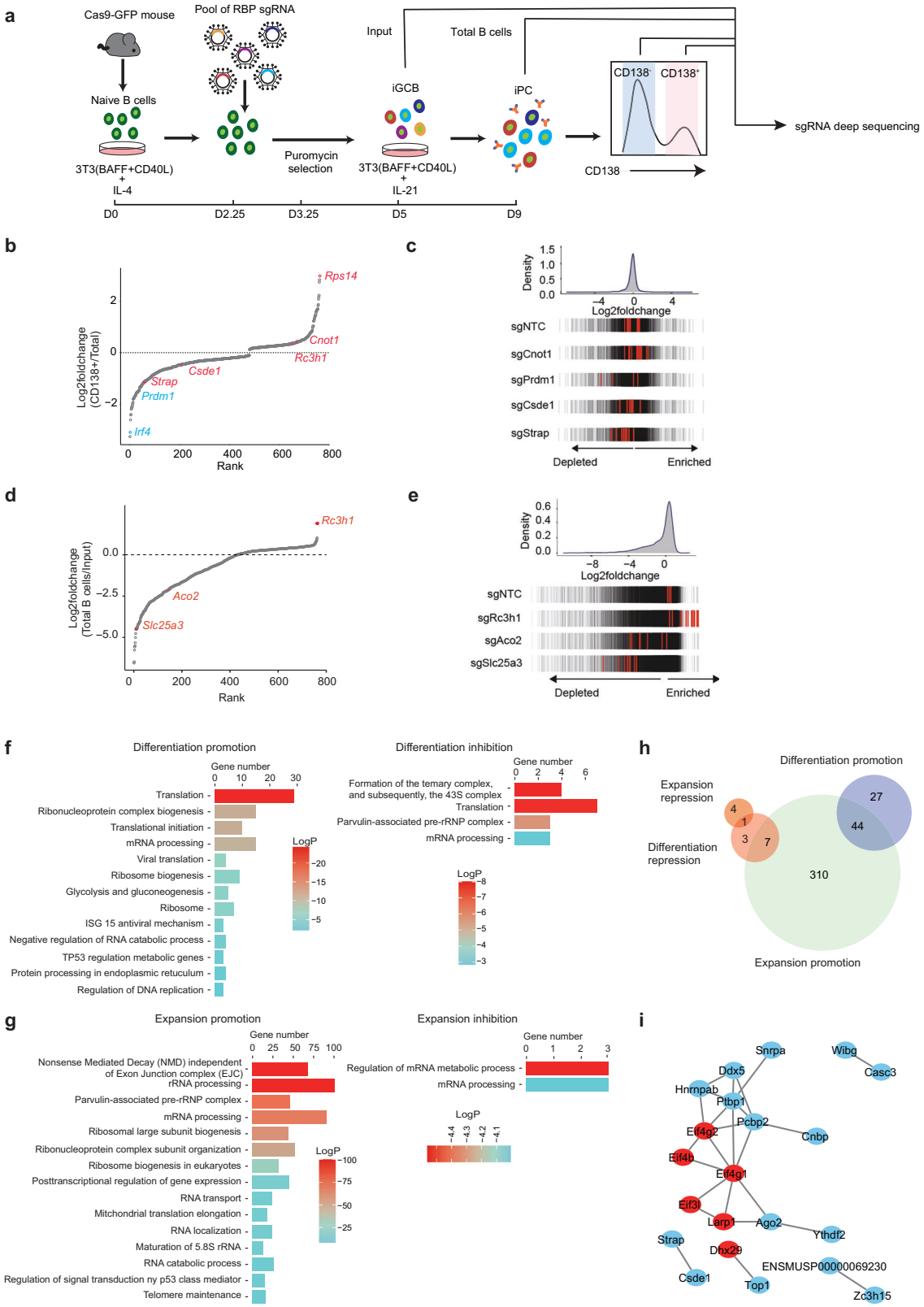

We then used Cas9⁺ B cells for the pooled sgRNA screening. As shown in Fig. 2a, Cas9⁺ B cells were infected with the pooled retroviral sgRNA library at a multiplicity of infection (MOI) of less than 0.2 to ensure that only one sgRNA was introduced into each cell. After puromycin selection, surviving cells were harvested and re-plated on fresh 40LB cells with IL-21 for plasma cell differentiation. A portion of survived cells were saved as input. After 4 days of culture with IL-21, cells were sorted by flow cytometry into CD19⁺CD138⁻ and CD19⁺CD138⁺ populations, as well as total B cells (CD19⁺), followed by sgRNA deep sequencing (Fig. 2a).

The quality of total read coverage and reproducibility of the screening samples were adequate for further data analysis (Supplementary Fig. 3g,h). To identify positive hits, the relative enrichment of sgRNAs between samples was computed by MAGeCK (model-based

Fig. 2 | CRISPR/Cas9-mediated functional analysis of RBPs regulating plasma cell differentiation. a Workflow for CRISPR/Cas9-mediated functional screening of RBPs in the iGCB culture system. b–e) Enrichment plot for differentiation (**b**, **c**) and expansion (**d**, **e**) screening. **b**, **d** The Y-axis shows log2 fold change (LFC) (CD138+ vs total B cells in (**b**) and total B cells vs input in **d**) of genes calculated from MAGECK. X-axis shows rank of genes by log2 fold change (LFC). Hits of interest and positive controls are highlighted in red and blue, respectively. **c**, **e** Distribution of log2-foldchange (CD138+ vs total B cells in (**c**) and total B cells vs input in (**e**) of all sgRNAs. sgRNAs targeting Cnot1, Prdm1, Csde1, and Strap are shown as examples for differentiation screening (**c**), while sgRNAs targeting Rc3h1, Aco2, and Slc25a3 are shown as examples for expansion screening (**e**). Histogram shows distribution of all sgRNAs. Red bars indicate sgRNAs targeting indicated genes, gray bars indicate all other sgRNAs. NTC, non-targeting control. **f**, **g** Enrichment analysis by Metascape for positive hits of screening. The *q*-value is an adjusted *p*-value corrected by the Benjamini-Hochberg procedure. **h** Venn diagram summarizing the overlap of differentiation and expansion regulators. See also Supplementary Data 7. **i** The protein-protein interaction analysis from STRING database shows enriched complexes of differentiation regulators (hits). Regulators of translation initiation are depicted as red circles.

analysis of genome-wide CRISPR-Cas9 knockout)[34]. In total, sgRNAs targeting 71 positive regulators of B cell differentiation were found depleted and sgRNAs targeting 11 negative regulators of B cell differentiation were found enriched in the CD138$^+$ population compared to total B cells (Fig. 2b, c, h; Supplementary Fig. 4b; Supplementary Data 5). By comparing total B cells with input, we identified 361 and 5 RBP genes that promote and inhibit cell expansion, respectively (Fig. 2d, e, h; Supplementary Fig. 4a; Supplementary Data 6). Notably, 366 of 759 RBPs regulated cell expansion, while only 82 of them regulated differentiation, with some regulating both expansion and differentiation (Fig. 2h; Supplementary Data 7). This is consistent with previous studies showing that B cell differentiation is coupled with expansion[35] and that only a small number of genes regulate CD4$^+$ T cell differentiation without any effect on proliferation[36].

As expected, we identified genes known to regulate B cell expansion (c-*Myc* and *Irf4*) and differentiation (*Prdm1, Irf4, Bach2*) (Supplementary Fig. 4a,b)[37,38]. *R3ch1*, an RBP known to inhibit B cell expansion, was also identified (Fig. 2d, e and Supplementary Fig. 4a)[16]. This demonstrates that our screening is robust and able to capture known regulators of B cell expansion and differentiation and that it should also be able to uncover new regulators of these cellular processes. Moreover, non-canonical and new RBPs identified by RIC were shown to play important roles in B cell expansion and/or differentiation (Supplementary Fig. 4c,d; Supplementary Data 8).

We performed GO analysis of positive hits to map core biological programs regulating B cell expansion and differentiation and discovered a profound enrichment of RBPs involved in translation among differentiation regulators (Fig. 2f, g). RBPs promoting B cell expansion were also enriched with functional clusters regulating mRNA translation and decay (Fig. 2f, g). Protein-protein interaction analysis of positive hits was performed to identify RBP complexes involved in B cell expansion and/or differentiation. RBP complexes regulating mRNA stability and translation including mitochondrial translation were found to be enriched (Supplementary Fig. 5).

Among the 82 RBPs that regulate plasma cell differentiation, 52 also regulate cell expansion, which includes cellular proliferation and survival (Fig. 2h). We performed protein-protein interaction analysis based on STRING databases of the other 30 RBPs that mainly regulate differentiation to see whether they function as protein complexes (Fig. 2i)[39]. 13 RBPs form a protein complex with some of them known to regulate translation initiation. A few others form smaller protein complexes. Among them are Ythdf2, Eif3l, Strap, and Csde1, which were identified as regulators of plasma cell differentiation in a recently published CRISPR/Cas9 screening of RBPs[40]. Mouse genetic studies showed that Ythdf2-deficient B cells exhibit deficient formation of GCB and plasma cell[40,41]. It is likely that other RBPs among those 30 also play critical roles in germinal center response and plasma cell differentiation.

Strap and Csde1 are important regulators of plasma cell differentiation

We focused on validating the 82 RBPs that regulate plasma cell differentiation (Fig. 2h). A few ribosomal proteins, such as Rps14, Rps3a, and Rps26, were excluded from validation for their known functions in ribosome. We cloned individual sgRNAs targeting the other 70 RBP genes into the same retroviral vector used in the sgRNA library screening. Naïve B cells from Rosa26-Cas9-GFP (CD45.2$^+$) and wild type (CD45.1$^+$) mice were cultured following experimental outline shown in Fig. 3a and analyzed by flow cytometry. The percentage of Cas9-GFP$^+$CD45.1$^-$ cells among total B cells indicates the effect of sgRNA on expansion, which includes cellular proliferation, survival, and death, while the percentage of CD19$^+$CD138$^+$ among Cas9-GFP$^+$CD45.1$^-$ cells indicates the effect of sgRNA on plasma cell differentiation (Fig. 3a and Supplementary Fig. 6).

As shown in Fig. 3b, c, deletion of 15 RBP genes showed significant effect on B cell expansion, plasma cell differentiation, or both. Notably, those RBPs fall into two main functional groups. The first group consisted of 8 RBPs regulating mRNA translation and decay. Eif4g2, Eif5a, and Eif3l are well known translation initiation and elongation factors[42–44]. Csde1, which forms a protein complex with Strap, regulates IRES-dependent translation initiation, as well as coding region instability determinant (CRD)-mediated translation and decay of *c-fos* mRNA[45]. Strap is a multifaceted protein that interacts with Csde1 and functions as a subunit of the SMN complex, but does not have well-defined RNA-binding domains[46,47]. Dhx9 is an RNA helicase participating in (CRD)-mediated translation and decay of *c-Myc* mRNA[48]. *Rc3h1*, which encodes Roquin, regulate deadenylation and degradation of its target mRNA[49]. Cnot1 is involved in mRNA deadenylation[50], miRNA-mediated repression, and translational repression[51].

The second group consisted of 6 RBPs functioning as metabolic enzymes and transporters. Eral1 and Aco2 function as enzymes in the mitochondrion[52,53], while Slc25a3 catalyzes the transport of phosphate into the mitochondrial matrix. Ldha and Gpi function as glycolytic enzymes[54,55]. Sec63 is a transporter mediating polypeptide transportation across the endoplasmic reticulum (ER) membrane[56]. The 15th RBP is Ubb, which encodes ubiquitin and targets cellular proteins for degradation by the 26S proteosome[57].

The functions of most of those RBPs in B cells have not been explored before, nor the RNA-binding ability of RBPs in the second group except Eral1. Our GO enrichment analysis of RBPs captured by RIC in iGCB and iPC cells, as well as RBPs identified by CRISPR/Cas9-mediated functional screening to regulate B cell expansion and/or plasma cell differentiation, indicated the involvement of mRNA translation and decay in controlling plasma cell differentiation (Supplementary Fig. 2d, e and Fig. 2f, g). Previous studies reported that Csde1 regulates mRNA translation and decay and that Csde1 forms a protein complex with Strap[58,59]. We therefore focused on Csde1 and Strap for further functional and mechanistic analyses. As shown in Fig. 3b, c and Supplementary Fig. 6, deletion of *Csde1* significantly inhibited plasma cell differentiation without much effect on expansion, suggesting a specific role in differentiation. Deletion of its interaction partner Strap showed comparable effect on plasma cell differentiation, with additional effect on expansion. The expression of Csde1 and Strap proteins were examined in wild type B cells during in vitro plasma cell differentiation. The expression of both proteins was low in naïve B cells, induced at day 1, and sustained during both stages of culture (Fig. 3d). In contrast, Prdm1 protein was significantly induced upon plasma cell differentiation, while Bach2 protein was

https://doi.org/10.1038/s41467-025-58212-8

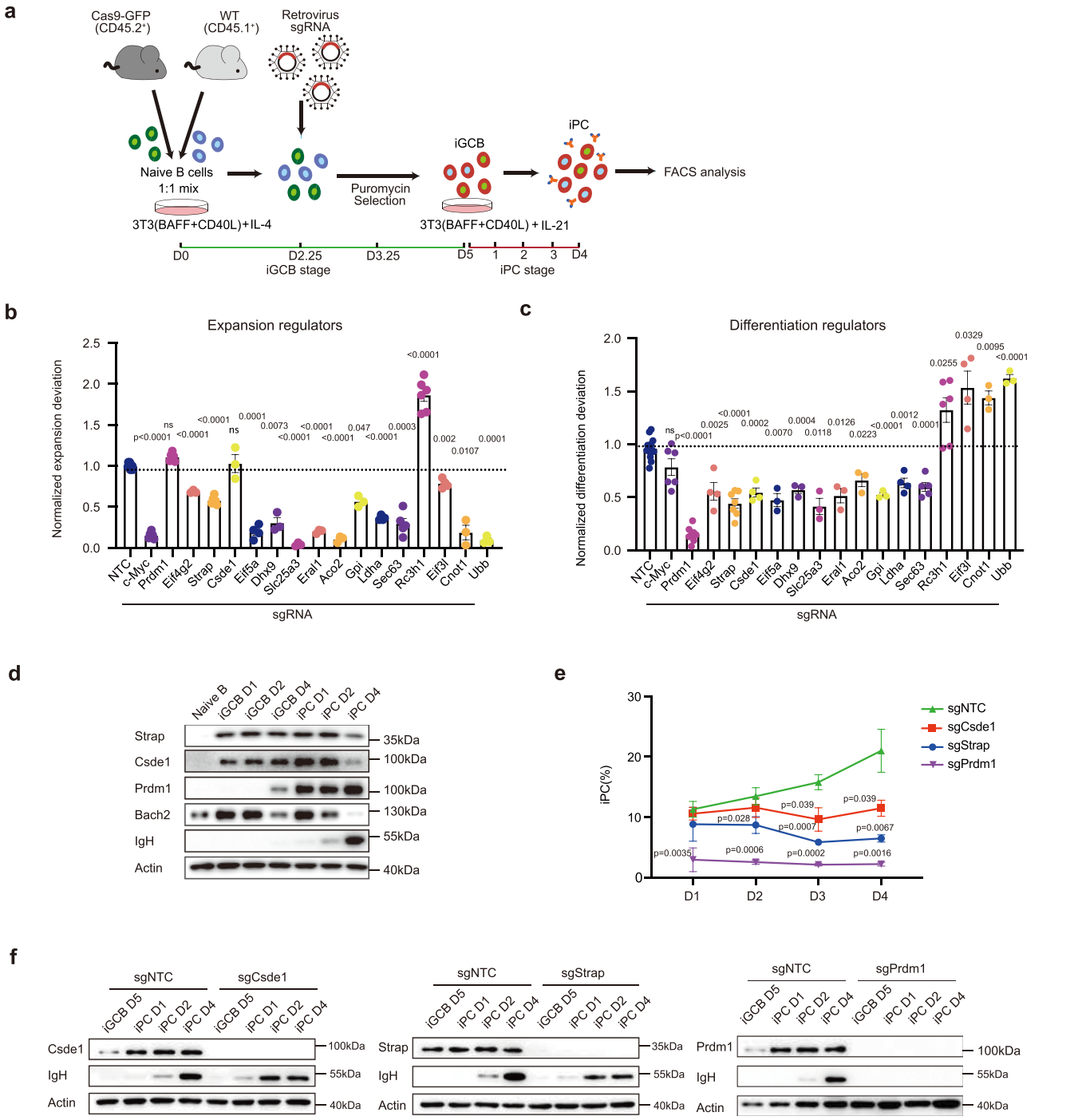

Fig. 3 | Strap and Csde1 are identified as critical regulators of plasma cell differentiation. a Workflow for validating individual hits from CRISPR screening in the iGCB culture system. Bar graphs summarizing the effect of sgRNAs targeting indicated genes (1–2 sgRNAs per gene) on B cell expansion (**b**) and differentiation (**c**). Expansion deviation is calculated as percentage of CD45.2$^+$ cells among total B cells/50%. Differentiation deviation is calculated as percentage of plasma cells among CD45.2$^+$ cells/percentage of plasma cells among CD45.1$^+$ cells. Data represent mean ± SEM of biological replicates (n = 12/6/6/3/6/3/4/3/3/3/3/3/4/5/6/4/3/3 from left to right). Statistical analyses were performed using unpaired two-tailed Student's t-test between non-targeting control (NTC) and sgRNA targeting indicated genes (ns, not significant). Source data is provided in a Source Data file. **d** Immunoblot analysis of protein expression at indicated time points during in vitro plasma cell differentiation of wild type B cells. **e** Flow cytometry analysis of percentage of CD19$^+$ CD138$^+$ iPC cells during in vitro plasma cell differentiation of B cells targeted by indicated sgRNAs. n = 3 biological replicates. Data represent mean ± SD. Statistical analyses were performed using multiple t-test (ns, not significant). Source data is provided in a Source Data file. **f** Immunoblot analysis of protein expression during in vitro plasma cell differentiation of B cells targeted by indicated sgRNAs.

present in naïve B cells and exhibited a bimodal expression pattern (Fig. 3d). The effect of sgRNAs on Csde1 and Strap proteins, as well as plasma cell differentiation, was examined at various time points during in vitro plasma cell differentiation (Fig. 3e, f). As shown in Fig. 3f, the depletion of Csde1 and Strap proteins was complete at iGCB day 5 and sustained throughout the iPC stage of culture. The detrimental effect of *Csde1* and *Strap* knockout on plasma cell differentiation started to manifest on iPC day 1 and became increasingly obvious afterwards,

accompanied by significant reductions in IgH protein levels (Fig. 3e, f). Therefore, Csde1 and Strap play critical roles during in vitro plasma cell differentiation.

Strap and Csde1 are essential for T cell-dependent antibody response

To investigate the role of Csde1 and Strap in the humoral immune response in vivo, we generated loxP-site flanked alleles of *Strap* and *Csde1* (Supplementary Fig. 7a,b), and crossed those mice with *Cγ1*-Cre mice, in which Cre expression is turned on upon B cell activation[60]. The development of both B and T cells are normal in the bone marrow and spleen of *Csde1*$^{fl/fl}$;*Cγ1*-Cre and *Strap*$^{fl/fl}$;*Cγ1*-Cre mice (Supplementary Fig. 8). There are no differences in germinal center B and plasma cells between unimmunized mutant and control mice (Supplementary Fig. 9a, b, c). Naive B cells from *Csde1*$^{fl/fl}$;*Cγ1*-Cre and *Strap*$^{fl/fl}$;*Cγ1*-Cre mice were cultured in vitro for plasma cell differentiation (Supplementary Fig. 7c). Consistent with sgRNA-mediated deletion, *Csde1*- and *Strap*-deficient B cells showed decreased plasma cell differentiation (Supplementary Fig. 7d, e). *Csde1*$^{fl/fl}$;*Cγ1*-Cre and *Strap*$^{fl/fl}$;*Cγ1*-Cre mice were immunized with 4-hydroxy-3-nitrophenyl hapten conjugated to ovalbumin (OVA) precipitated in alum together with lipopolysaccharide (NP-OVA/Alum/LPS), a T cell-dependent antigen (Fig. 4a). GCB and plasma cells in the spleen were analyzed by flow cytometry at day 14 post immunization (Fig. 4b, c and Supplementary Fig. 9a). The percentage and number of germinal center B cells decreased significantly in both *Strap*$^{fl/fl}$;*Cγ1*-Cre and *Csde1* $^{fl/fl}$;*Cγ1*-Cre mice. While the percentage and number of total plasma cells were only slightly changed, NP-specific IgG1$^+$ plasma cells were drastically reduced in both *Strap*$^{fl/fl}$;*Cγ1*-Cre and *Csde1*$^{fl/fl}$;*Cγ1*-Cre mice (Fig. 4b,c). Consistently, those mutant mice exhibited much decreased number of NP-specific IgG1$^+$ antibody-secreting cells (ASCs) in the spleen (Supplementary Fig. 9d, e). We next immunized WT, *Strap*$^{fl/fl}$;*Cγ1*-Cre and *Csde1*$^{fl/fl}$;*Cγ1*-Cre mice with 4-hydroxy-3-nitrophenyl hapten conjugated to ovalbumin (OVA) precipitated in alum (Fig. 4d). Enzyme Linked Immunosorbent Assay (ELISA) analysis showed a significant reduction in the serum concentration of NP-specific IgG1 antibody, with marginal effect on NP-specific IgM which didn't undergo affinity maturation upon T-cell dependent immune response (Fig. 4e). Taken together, these findings demonstrate that Strap and Csde1 play essential roles in germinal center reaction, plasma cell differentiation and affinity-maturated antibody production. The highly similar phenotypes of *Strap*$^{fl/fl}$;*Cγ1*-Cre and *Csde1*$^{fl/fl}$;*Cγ1*-Cre mice suggest that those two RBPs work together to control T cell-dependent antibody response.

Identification of Csde1 and Strap targets by eCLIP-Seq

We next performed eCLIP-seq analysis of wild type iPC cells to identify mRNA targets of Csde1 and Strap to gain insights into the molecular mechanisms underlying their regulation of plasma cell differentiation (Fig. 5a)[61]. Both Csde1 and Strap proteins are predominantly localized in the cytosolic fractions of day 2 iPC cells (Supplementary Fig. 10a). We examined the precipitation efficiency of Csde1 and Strap antibodies, as well as the size distribution of the co-precipitated RNA fragments crosslinked with RBP by UV (termed RNA-RBP complexes hereafter) using RNA-imaging. Notably, Csde1 and Strap proteins remained associated with each other following the stringent washing of the eCLIP procedure (Supplementary Fig. 10b). For canonical RBPs, the RNA fragments crosslinked with RBP often appear in the 75KD range above the RBP on SDS-PAGE gel. However, the RNA-RBP complexes precipitated by either Csde1 or Strap antibodies appeared in the range of 42–260 KD (Supplementary Fig. 10c). This is interesting, considering that the molecular weights of Csde1 and Strap proteins are 38 and 89KD, respectively. We speculated that both Csde1 and Strap are able to bind RNA directly, that Csde1 and Strap remained bound to each other throughout the eCLIP procedure, and that immunoprecipitation of any one of these two proteins pulled down the other, as well as RNA fragments crosslinked with them, resulting in similar RNA-imaging results.

The RNA fragments precipitated by both Csde1 and Strap antibodies were sequenced. Biological replicates showed high reproducibility (Supplementary Fig. 10d). 10132 and 7171 peaks were identified for Csde1 and Strap, respectively (Fig. 5b). The peak distribution was analyzed and the metagene plots were generated by size-normalizing binding across all protein-coding transcripts. Intriguingly, the patterns of peak distribution for Csde1 and Strap were highly similar. Most peaks were distributed in coding sequence (CDS) regions, with a small portion of peaks in the 5′ and 3′ UTR regions (Fig. 5b,c). We wondered whether Csde1 and Strap regulate RNA splicing during plasma cell differentiation. Peak numbers near the putative splicing sites were calculated in meta-intron plots and the mean coverage around the splicing sites was very low (Fig. 5d), thereby excluding the possibility that Csde1 and Strap regulate their target mRNAs through splicing. RBPs binding to CDS regions of target mRNAs were shown to regulate mRNA translation and decay[8,62,63], suggesting that Csde1 and Strap may regulate their target genes through those mechanisms.

The eCLIP-seq peaks of Csde1 and Strap were mapped to 1479 and 2289 target genes, respectively, among which were 444 common targets (Fig. 5e; Supplementary Data 9, 10). Csde1 and Strap binding sites on those common targets were further examined. 182 common targets harbor overlapping binding sites for Csde1 and Strap, while the other 262 common targets carry Csde1 and Strap binding sites in distinct regions of their mRNAs (Fig. 5e; Supplementary Data 11). We next analyzed the consensus binding motifs based on the eCLIP-seq results and found both similar and distinct binding motifs for Csde1 and Strap (Fig. 5f).

We performed GO enrichment analysis of target genes identified by eCLIP-seq to explore biological processes regulated by Csde1 and Strap. Genes associated with "lymphocyte differentiation" and "B cell receptor signaling pathway" were enriched among the Csde1 target genes, while genes associated with "cellular responses to stress" and "translation" were enriched among the Strap target genes (Fig. 5g). There were many gene sets shared by Strap and Csde1, especially "adaptive immune system", suggesting that they may regulate some common processes of B cell immune responses.

Strap and Csde1 regulate B cell differentiation through common targets

We performed quantitative mass spectrometry analysis of wild type (WT), *Csde1*$^{fl/fl}$;*Cγ1*-Cre (Csde1 KO), and *Strap*$^{fl/fl}$;*Cγ1*-Cre (Strap KO) day 1 iPC cells to investigate the effect of Csde1 and Strap deficiency on the proteome, as well as on the protein levels of their target genes (Supplementary Data 12). As shown in Fig. 6b and Supplementary Data 13, protein products of 8134 genes were quantified, including 352 of the 444 common targets for Csde1 and Strap (Fig. 5e). Principal component analysis (PCA) showed that the proteomes of Csde1 and Strap KO cells clustered together and were significantly different from that of WT cells (Fig. 6a). Consistent with PCA results, genome-wide protein changes caused by *Csde1* and *Strap* deficiency presented excellent correlation, while correlation of protein changes of common target genes was even better (Fig. 6d; Supplementary Data 14), suggesting that these two RBPs regulate common biological processes through common target genes. GO enrichment analysis of genes whose protein levels were significantly changed in Csde1 and Strap KO cells also showed high correlation in those two types of cells. Notably, genes associated with "protein processing in endoplasmic reticulum" and "cholesterol metabolism" were significantly downregulated in protein levels in both Csde1 and Strap KO cells (Fig. 6c). A recent study reported that these two cellular processes play essential roles in plasma cell differentiation[64]. Therefore, downregulation of genes regulating those cellular processes is consistent with impaired T cell-dependent antibody response in *Strap*$^{fl/fl}$;*Cγ1*-Cre and *Csde1*$^{fl/fl}$;*Cγ1*-Cre mice (Fig. 4).

https://doi.org/10.1038/s41467-025-58212-8

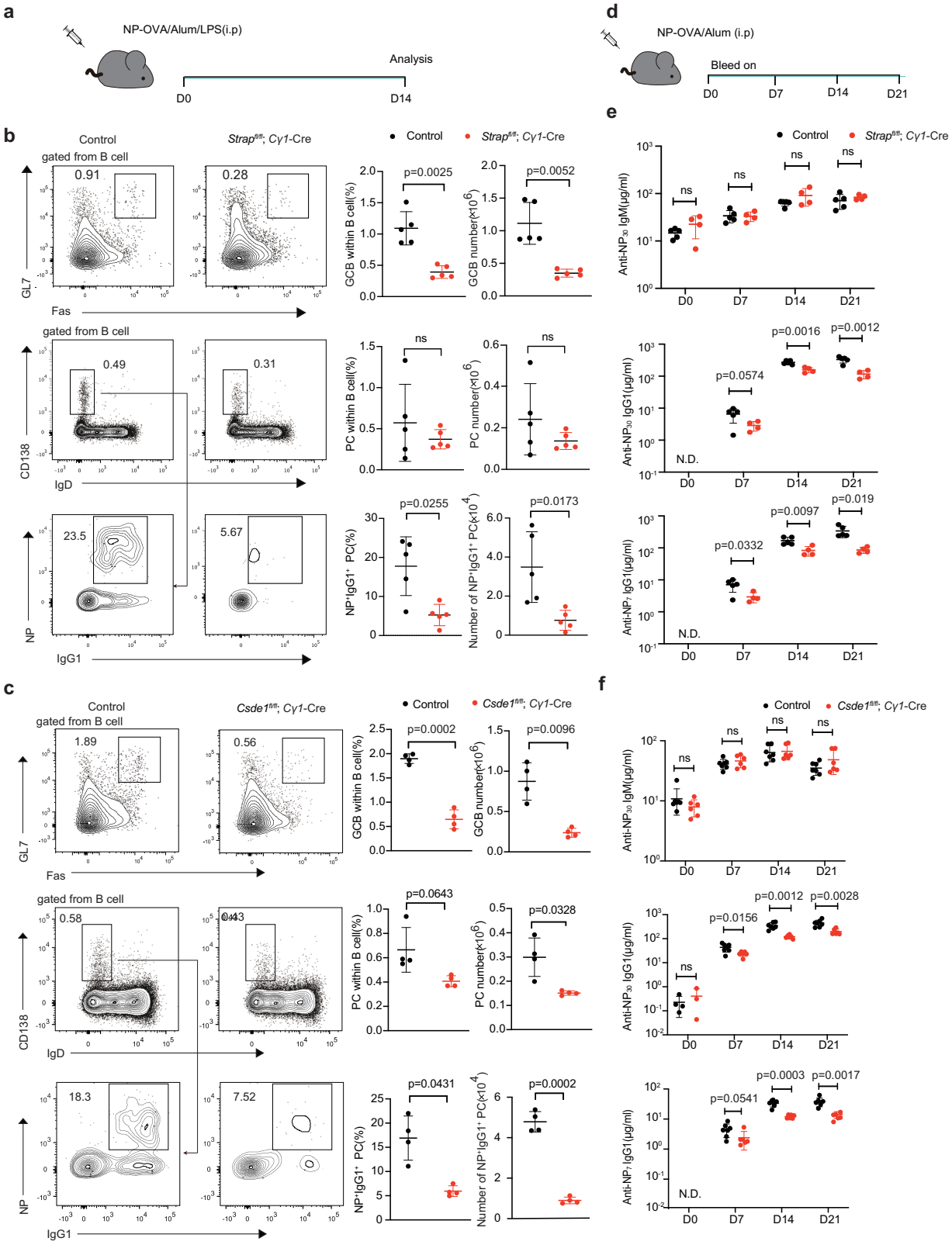

We then focused on protein changes in common target genes. Among the 352 common target genes whose proteins were quantified, 29 showed significant changes in both Csde1 and Strap KO cells (Fig. 6e). Those genes were termed differentially expressed targets (DETs). Metascape enrichment analysis showed genes associated with "B cell differentiation" were highly enriched among the 29 common DETs (Fig. 6f). Changes in protein levels of those 29 genes in Csde1 and Strap KO cells were plotted in a heatmap, which revealed increased protein levels of Bach2, Irf8, Pou2f2, and Ighm, as well as decreased protein levels of Atp2a2, Herpud1 and CD79b in Csde1 and Strap KO cells (Fig. 6g). Excessive Bach2[38], Irf8[65] and Pou2f2[66] or loss of Atp2a2[67] had been shown to inhibit plasma cell differentiation, suggesting that Strap and Csde1 regulate plasma cell differentiation through these common targets.

Fig. 4 | Strap and Csde1 are essential for T cell-dependent antibody response. **a** Schematic representation of the immunization experiment. Mice were 2–3 month old. Flow cytometry analysis of splenic GCB, plasma cells (PC) and NP-specific PC in the spleen of *Strap*$^{fl/fl}$;*Cγ1*-Cre (**b**) ($n = 5$ per group. KO group had 4 males and 1 female while control group had 3 males and 2 females.) and *Csde1*$^{fl/fl}$;Cγ1-Cre (**c**) ($n = 4$ per group. Both KO group and control group had 1 male and 3 females.) mice at day14 after immunization with NP-OVA(50ug)/Alum/LPS(10ug). Statistical analyses summarizing the percentage and number of indicated populations. **d** Schematic representation of the immunization experiments for ELISA. Serum was collected at indicated time points. Mice were 2–3 month old and all were females. *Strap*$^{fl/fl}$; *Cγ1*-Cre ($n = 4$) and control mice ($n = 5$) (**e**), *Csde1*$^{fl/fl}$; *Cγ1*-Cre ($n = 6$) (**f**) and control mice ($n = 7$) (**f**) were immunized with NP-OVA(50ug)/Alum. Serum was collected at indicated time points as shown in d. ELISA analysis of NP-specific IgM, total (NP_{30}), and high affinity (NP_7) NP-specific IgG1 antibody. Each symbol represents an individual mouse. Data represent mean ± SD. Statistical analyses were performed using unpaired two-tailed Student's t-test (ns, not significant; N.D., not detected). Source data is provided in a Source Data file.

Bach2 and Atp2a2 mediate Csde1 and Strap regulation of plasma cell differentiation

We next assessed the functional contribution of those 29 common target genes to Strap and Csde1 regulation of plasma cell differentiation. For target genes upregulated in Csde1 and Strap KO cells, we introduced sgRNAs targeting them individually, together with sgRNAs targeting Csde1 or Strap, into Cas9-GFP B cells in the in vitro plasma cell differentiation system (Fig. 7a). As shown in Fig. 7b,c and Supplementary Fig. 11, *Bach2* deletion significantly restored plasma cell differentiation of *Csde1*- and *Strap*-deficient cells. This is accompanied by impaired cell expansion, consistent with a role of Bach2 in promoting B cell proliferation and survival[68]. Immunoblot analysis showed that Bach2 protein level was significantly elevated in *Csde1*- and *Strap*-deficient cells and was brought back to the control level in double knockout cells (sgStrap/sgCsde1+sgBach2) (Fig. 7d). Consistent with restored plasma cell differentiation, Prdm1 protein level was also restored by *Bach2* deletion in *Csde1*- and *Strap*-deficient cells (Fig. 7d). Furthermore, ectopic expression of Bach2 significantly reduced Prdm1 protein level and impaired plasma cell differentiation (Fig. 7e). These results demonstrate that Bach2 is a major downstream effector of Csde1 and Strap in regulating plasma cell differentiation.

For target genes downregulated in Csde1 and Strap KO cells, sgRNAs were designed to knockout them in Cas9-GFP B cells. As shown in Fig. 7f and Supplementary Fig. 12, deletion of Atp2a2 significantly inhibited expansion and plasma cell differentiation of Cas9-GFP B cells, while deletion of other target genes had little effect on plasma cell differentiation. Immunoblot analysis confirmed the reduced protein level of Atp2a2, as well as Prdm1, by sgRNA targeting Atp2a2 (Fig. 7g). Moreover, ectopic expression of Atp2a2 partially restored plasma cell differentiation of Csde1 and Strap KO B cells (Fig. 7h, i and Supplementary Fig. 13a-c). Taken together, these results suggest that *Atp2a2* plays an important role in mediating Strap and Csde1 regulation of plasma cell differentiation.

We further examined the effect of Csde1 and Strap-deficiency on the protein and mRNA levels of themselves, Bach2, Atp2a2, Prdm1 and IgH during plasma cell differentiation (Fig. 7j, k and Supplementary Fig. 13d, e). The *Atp2a2* mRNA levels were similar in WT, Csde1 KO, and Strap KO cells in early stage of iPC differentiation, while Atp2a2 protein levels were constantly lower in Csde1 and Strap KO than WT cells (Fig. 7j, k), suggesting that Csde1 and Strap mainly regulate the synthesis and/or degradation of Atp2a2 protein.

A recent study suggests that Bach2 protein expression kinetics controls B cell fate[13]. As shown in Fig. 7j, k and Supplementary Fig. 13d, e, at the beginning of iPC differentiation, iGCB day 4 cells expressed significant amount of Bach2 mRNA but little Bach2 protein. CD40 and IL-21 signals induced a rapid and transient upregulation of Bach2 protein, accompanied by quick downregulation of *Bach2* mRNA. In the absence of Csde1 or Strap, the downregulation of *Bach2* mRNA was attenuated, accompanied by elevated and prolonged expression of Bach2 protein, which impaired plasma cell differentiation. We speculate that elevated Bach2 protein level in Csde1 and Strap KO cells is caused by active translation induced by CD40 and IL-21 signals in combination with attenuated downregulation of *Bach2* mRNA.

Csde1 and Strap regulate translation and decay of target mRNAs

Polysome profiling analysis of WT, Csde1 KO, and Strap KO day 1 iPC cells showed they exhibited the same global polysome distribution, suggesting that Csde1 and Strap-deficiency did not cause global changes in mRNA translation (Supplementary Fig. 14a). We performed ribosome profiling (RP) and parallel RNA-seq analysis of these cells to elucidate molecular mechanisms underlying Csde1 and Strap regulation of their target genes (Fig. 8a)[69]. Employing an R package named deltaTE[70], we divided the differential expressed genes into 4 modes: forwarded, exclusive, intensified, and buffered (Supplementary Fig. 14b, Supplementary Data 15). In the 'forwarded' regulation mode, genes are mainly regulated at the mRNA level and are termed differentially transcribed genes (DTG). In the other three regulation modes, 'exclusive', 'intensified', and 'buffered', genes are regulated at the translational level and are defined as differential translation efficiency (TE) genes (DTEG). Among those DTEGs, most are regulated by the 'buffered' mode (Supplementary Fig. 14b).

As we have shown in Fig. 6d, protein abundance changes were highly correlative in Csde1 and Strap KO iPC cells. We wondered whether ribosome footprint changes in those cells were also similar, especially for common target genes. While there was no obvious correlation in genome-wide ribosome footprint changes in Csde1 and Strap KO cells, common target genes showed certain degree of correlation. The correlation was even higher for the 29 common differentially expressed targets (DETs) (Fig. 8b). We further examined mRNA levels and ribosome footprints of those common target genes (Fig. 8c, Supplementary Data 16, 17). Among them, Atp2a2 is regulated by the 'intensified' mode, namely that there was a slight decrease in the Atp2a2 mRNA level, while the overall decrease in the Atp2a2 ribosome footprint was "intensified" in Csde1 and Strap KO cells. As shown in Fig. 7j, k, and Fig. 8c, Csde1- and Strap-deficiency had little effect on the mRNA level but caused a significant reduction in the protein level of Atp2a2, likely due to decreased translation efficiency. Indeed, there was a slight shift of *Atp2a2* mRNA towards light polysome fractions in polysome profiles of Csde1 and Strap KO cells, indicating reduced translation rate (Supplementary Fig. 15a).

Interestingly, Bach2 is regulated by the "buffered" mode, namely that there was a significant increase in the *Bach2* mRNA level, while the overall increase in the Bach2 ribosome footprint was "buffered" in Csde1 and Strap KO cells, likely by decreased translation efficiency (Fig. 8c). This buffering effect can be found for many common targets regulated by Strap and Csde1, as there was a clear negative correlation between changes in their mRNA levels and translation efficiency (Supplementary Fig. 14c). As the downregulation of Bach2 mRNA was attenuated in Strap and Csde1 KO cells (Fig. 7k), we speculated that Strap- and Csde1-deficiency increased the stability of Bach2 mRNA.

Indeed, the half-life of Bach2 mRNA was significantly prolonged in Strap and Csde1 KO cells stimulated by CD40L, BAFF and IL-21 (Fig. 8d). Previously studies reported that Csde1 promotes translationally coupled decay of *c-Fos* mRNA, which harbors a major protein coding-region determinant of instability (mCRD), a purine-rich region responsible for Csde1-mediated translation-induced mRNA decay[45]. Similarly, Csde1 binds to a purine-rich sequence in the CDS region of *Bach2* mRNA, while Strap binds to its 3' UTR region near the stop

https://doi.org/10.1038/s41467-025-58212-8

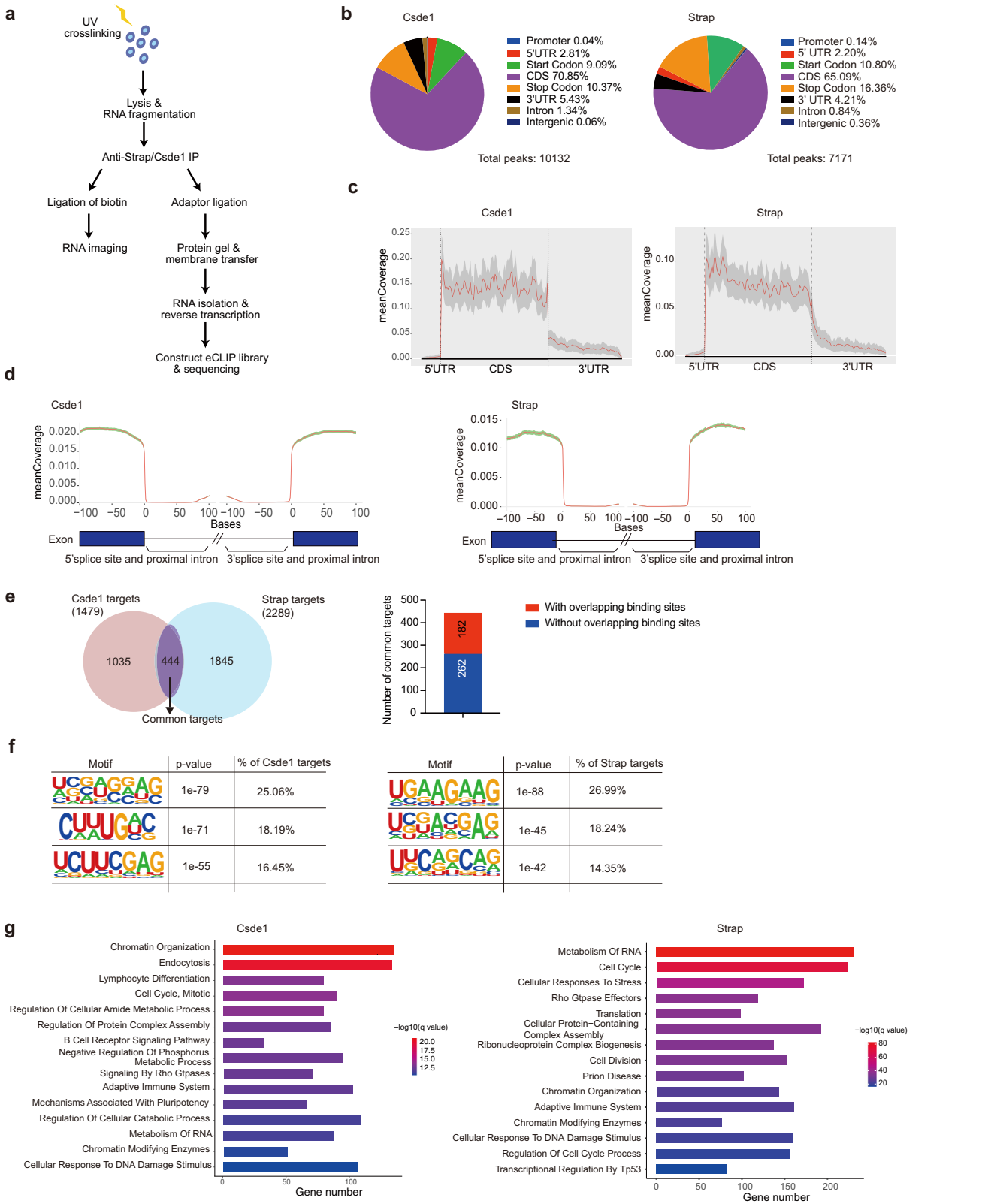

Fig. 5 | Identification of Csde1 and Strap targets by eCLIP-Seq. a Schematic representation of the eCLIP-Seq experiment. **b** Pie charts summarizing the distribution of peaks on genomic regions identified as targets of Csde1 and Strap by eCLIP-seq. **c** Meta-gene profiles of mean coverage of reads in mRNAs identified as targets for Csde1 and Strap by eCLIP-seq. Data represent mean ± SE. **d** Meta-exon plots summarizing distribution of peaks targeted by Csde1 and Strap within the displayed regions (100 nucleotides of intron and 100 nucleotides of exon flanking the 5′ and 3′ splicing sites). **e** Venn diagram summarizing common target genes of Csde1 or Strap identified by eCLIP-seq. The histogram categorizes those common targets based on the presence/absence of overlapping binding sites. **f** The top 3 most enriched motifs in peaks identified by eCLIP-seq for Csde1 and Strap target genes. Statistical analyses were performed through either the cumulative hypergeometric or cumulative binomial distributions. **g** GO analysis of Csde1 and Strap target genes.

https://doi.org/10.1038/s41467-025-58212-8

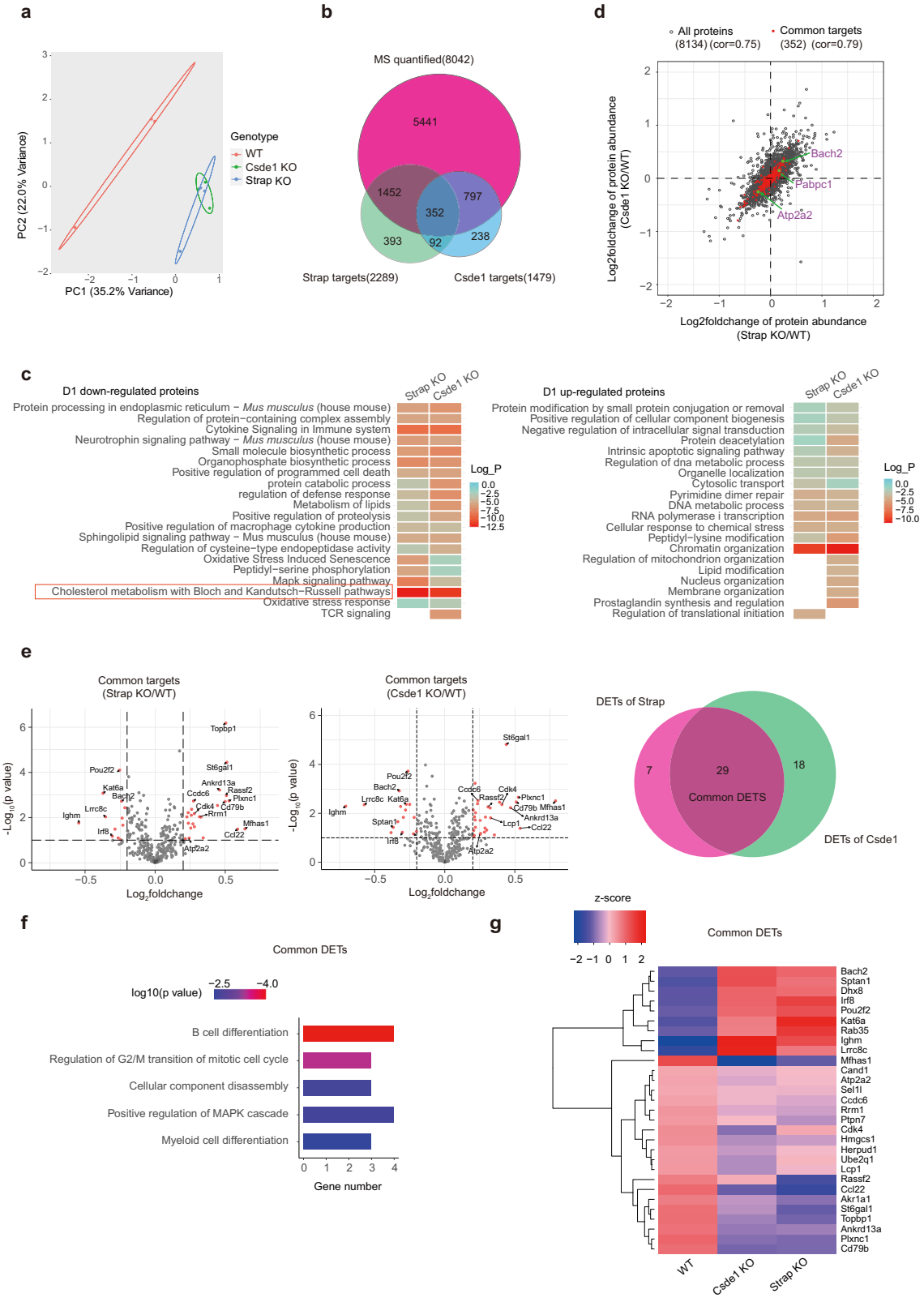

codon (Supplementary Fig. 15b). Those binding regions are evolutionarily conserved, suggesting their functional importance (Supplementary Fig. 15c). We speculate that Csde1 and Strap binding to the *Bach2* mRNA mediates translation-induced decay of *Bach2* mRNA in response to CD40L and IL-21 stimulation. As previously reported[13], the low Bach2 protein expression in day 4 iGCB cells was likely caused by inefficient translation initiation due to the presence of GC-rich complex secondary structures in the 5′UTR of *Bach2* mRNA. Upon CD40L, BAFF and IL-21 stimulation, translation of *Bach2* mRNA is significantly increased in day1 iPC cells (Fig. 8e), leading to upregulation of Bach2 protein levels (Fig. 3e). Active translation may trigger translation-induced decay of *Bach2* mRNA, resulting in down-regulation of *Bach2* mRNA and, subsequently, protein levels. Consistent with this hypothesis, when WT iGCB cells were stimulated by

Fig. 6 | Strap and Csde1 regulate B cell differentiation through some common targets. a Principal component analysis (PCA) analysis of proteomes of WT, Csde1 cKO and Strap cKO day1 iPC cells quantified by mass spectrometry. **b** Venn diagram summarizing the overlap between all mass spectrometry (MS)-quantified genes, Csde1, and Strap targets. **c** GO analysis of genes with significant changes in protein levels in Strap KO and Csde1 KO cells. The *p*-value here is an adjusted *p*-value corrected by the Benjamini-Hochberg procedure. **d** Scatter plots depicting correlation of protein abundance changes in Strap KO and Csde1 KO cells. Gray dots, all MS-quantified proteins; red dots, MS-quantified common targets of Strap and Csde1. The correlation of X and Y values in all proteins and common targets was calculated. **e** Volcano plots summarizing differentially expressed targets (DETs) among common targets in Strap KO and Csde1 KO cells. Red dots indicate genes with log2foldchange > 0.2 and *p*-value < 0.1. Venn diagram showing common DETs from Strap KO and Csde1 KO cells. Statistical analyses for differentially expressed genes between conditions were performed through Wald test. The *p*-value was corrected by the Benjamini-Hochberg procedure. **f** GO enrichment analysis of common DETs. The *p*-value is an adjusted *p*-value corrected by the Benjamini-Hochberg procedure. **g** Heatmap of protein expression levels of 29 common DETs in WT, Csde1 KO, and Strap KO cells. Protein expression levels were z-score normalized. Source data is provided in the Source Data file.

CD40L and IL-21, inhibiting translation by cycloheximide (CHX) led to significant increase in *Bach2* mRNA levels (1.57-fold at 2 h and 3.29-fold at 4 h after stimulation). In contrast, Csde1 KO iGCB cells exhibited elevated *Bach2* mRNA levels, but CHX treatment resulted in no further increase at 2 h and only 2.31-fold increase at 4 h upon CD40L, BAFF and IL-21 stimulation (Fig. 8f). These results confirmed that *Bach2* mRNA level is controlled by translation-induced mRNA decay mechanisms, suggesting that Csde1 plays an important role in mediating translation-induced decay of *Bach2* mRNA. As a comparison, CD40L, BAFF and IL-21 stimulation did not promote translation of *Atp2a2* mRNA (Fig. 8e), and *Atp2a2* mRNA levels exhibited only marginal changes in response to cycloheximide treatment and Csde1-deficiency (Fig. 8f). Taken together, these results suggest an important role of Csde1 and Strap in coupling translation and decay of their target mRNAs.

We noticed that CD40L, BAFF and IL-21-induced translation and decay of *Bach2* mRNA occur rapidly in the first 24 h after stimulation. To assess the functional importance of the timing of this exquisite control of Bach2 expression, we restored the expression of Csde1 in Csde1 KO B cells at different time points of iGCB culture by controlling the timing of retroviral transduction (Supplementary Fig. 16a). When retroviruses encoding Csde1 were added at iGCB day 2.25, Csde1 protein was fully restored by iGCB day 4 and maintained at higher than WT levels afterwards (Supplementary Fig. 16d), leading to a quick downregulation of Bach2 protein by iPC day 2 and restored plasma cell differentiation (Supplementary Fig. 16b,c). Notably, when retroviruses encoding Csde1 were added at iPC day 1, Csde1 protein was not expressed until iPC day 2. Bach2 protein expression remained high at iPC day 2 and plasma cell differentiation was only marginally restored (Supplementary Fig. 16b-d). Therefore, during this highly dynamic process, Csde1- and Strap-mediated translation-induced mRNA decay taking place in the first 24 h seems to be essential for controlling the duration and magnitude of Bach2 protein upregulation, and this exquisite control of Bach2 protein expression kinetics plays a critical role in B cell fate determination.

Strap interaction is essential for Csde1 regulation of plasma cell differentiation

Previous studies showed that Csde1 and Strap form a protein complex[58,59,71], but the functional importance of this complex remains unclear. In this study, immunoprecipitation (Supplementary Fig. 10b), mouse genetics (Fig. 4), proteome analysis (Fig. 6a, d), and eCLIP analysis (Fig. 5) all suggest that Csde1 and Strap form a tightly associated functional complex and play similar roles in B cells. Furthermore, ectopic expression of Csde1 in Strap KO cells and ectopic expression of Strap in Csde1 KO cells were not able to restore plasma cell differentiation, excluding their functional redundancy (Fig. 7h and Supplementary Fig. 13b, c). We speculate that Csde1 and Strap regulate the translation and decay of their common target mRNAs in a highly cooperative manner and that the Csde1-Strap interaction is essential for their regulation of plasma cell differentiation.

The Csde1 protein consists of 5 CSD domains at the N-terminus and a SUZ-C domain at the C-terminus[59,72]. While the CSD domains are evolutionarily conserved RNA-binding domains, amino acids 744–757 of the Csde1 SUZ-C domain are homologous to the Strap-binding sequences found in other Strap binding proteins[73]. We generated a Csde1 mutant with the SUZ-C domain deleted (Csde1 Δc) (Fig. 9a) and introduced it into Csde1 KO iPC cells by retroviral transduction. As shown in Fig. 9b-d, Csde1 Δc did not interact with Strap and was not able to restore plasma cell differentiation of Csde1 KO cells, confirming the functional importance of the SUZ-C domain in binding Strap and regulating plasma cell differentiation. We further investigated the requirement of Strap interaction for Csde1 function by generating a Csde1 Δc mutant with Strap tethered to its C-terminus through a flexible glycine-serine linker (Csde1 Δc-Strap, Fig. 9a-c). Strikingly, Csde1 Δc-Strap was able to restore plasma cell differentiation of Csde1 KO cells to a large degree (Fig. 9d). Furthermore, retroviral expression of both Csde1 and Csde1 Δc-Strap was able to bring the expression of Bach2 and Atp2a2 proteins close to WT levels in Csde1 KO cells, while Csde1 Δc had little effect (Fig. 9b). We next investigated whether Csde1 and Strap affect each other's ability to bind target mRNAs. In the absence of Strap, Csde1 binding to target mRNAs was significantly impaired (Fig. 9e). Notably, Csde1 deficiency also abolished Strap binding to target mRNAs (Fig. 9e). Taken together, these findings demonstrate that Csde1-Strap interaction is crucial for their binding to target mRNAs and promoting plasma cell differentiation.

Discussion

In this study, we performed mRNA-interactome capture to systematically discover mRNA-associated RBPs in an in vitro culture system of plasma cell differentiation, demonstrating the existence of a group of core RBPs performing functions common to all cell types, a small number of cell type-specific RBPs, and some RBPs without known RNA binding domains. We also performed CRISPR/Cas9-mediated screen to identify functional RBPs among them. Through GO enrichment and protein-protein interaction analysis, RBPs regulating translation and mRNA stability, such as nonsense-mediated decay and CRD-mediated mRNA stabilization, were enriched among functional RBPs. Our study established the functional RBP landscape of the B cell immune response and illustrated the fundamental importance of regulating mRNA translation and decay during B cell fate determination.

Our CRISPR/Cas9-mediated functional analysis identified 15 RBPs that play significant roles in regulating B cell expansion, plasma cell differentiation, or both. Those RBPs mainly fall into two functional groups. The first group consisted of 8 RBPs regulating mRNA translation and decay. The second group consisted of 6 RBPs functioning as metabolic enzymes and transporters. The functions and RNA-binding ability of some of those RBPs in B cells are unknown, which warrant future investigations.

We dissected the functions and molecular mechanisms of actions of Csde1 and Strap in B cells. Mouse genetics studies showed that Csde1 and Strap play critical roles in T cell-dependent antibody responses. Employing eCLIP-seq, quantitative mass spectrometry, RNA-seq, and ribosome profiling, Csde1 and Strap were found to mainly bind to coding sequences of target mRNAs and regulate their translation and decay. Bach2 and Atp2a2 were identified as key targets of Csde1 and Strap during plasma cell differentiation. Notably, our multi-omics analysis revealed a striking negative correlation between

https://doi.org/10.1038/s41467-025-58212-8

changes in translation efficiency and expression levels of target mRNAs impacted by the deletion of Csde1 and Strap, suggesting that those two RBPs extensively regulate the abundance and translation of target mRNAs to exert exquisite control of protein expression. Our findings highlight the fundamental importance of precise control of protein expression kinetics of key regulators, Bach2 in this case, by multiple layers of regulatory mechanisms during B cell immune responses.

Csde1 was previously found to regulate the translation and decay of mRNAs of early response genes (ERGs), whose coordinated and transient expression accompanied the transition of cells from the resting state, G0, into the cell cycle[7]. c-Fos and c-Myc are ERGs whose protein expression is rapidly and transiently upregulated in response to stimulation[74,75]. Ribosomal transit through the major protein-coding region determinant of instability (mCRD) of c-fos mRNA triggers its

Fig. 7 | Bach2 and Atp2a2 mediate Csde1 and Strap regulation of plasma cell differentiation. a Experimental design for identifying functional target genes of Csde1 and Strap. Bar graphs summarizing the effect of sgRNAs targeting indicated genes on expansion and differentiation of B cells targeted by sgRNA against Csde1 (**b**) or Strap (**c**). Each gene was targeted by 1–2 sgRNAs. Data represent mean ± SD of independent biological replicates (n = 12/10/4/4/4/4/4/7/4/5 from left to right). Source data is provided in a Source Data file. Statistical analyses were performed using two-sided t-test between sgRNAs and non-targeting control (NTC) in B cells targeted by sgRNA against either Csde1 or Strap. **d** Immunoblot analysis of cells transduced with retroviruses encoding indicated sgRNAs. **e** WT B cells were transduced with retroviruses encoding Bach2 during iGCB culture. Bar graph summarizes percentages of CD138+ iPC cells. n = 3 independent biological replicates. Immunoblot analysis of indicated proteins in B cells transduced with empty retroviruses (vector) or retroviruses encoding Bach2. **f** WT Cas9$^+$ B cells were transduced with retroviruses encoding indicated sgRNAs during iGCB culture. Bar graphs summarize the effect of sgRNAs on B cell expansion and differentiation. Data represent mean ± SD of independent biological replicates (n = 8/5/4/2/2/4/3/2/4/2/3/2/4/2/3/2/3/2/4/2/2/2/4 independent biological replicates from left to right). sgRNAs effects were compared to NTC using two-sided t-test. Source data is provided in a Source Data file. **g** Immunoblot analysis of Atp2a2 in B cells targeted by indicated sgRNAs. **h**, **i** B cells from WT, *Csde1*$^{fl/fl}$;*Cγ1*-Cre (Csde1 KO), and *Strap*$^{fl/fl}$;*Cγ1*-Cre (Strap KO) mice were transduced with retroviruses encoding indicated proteins during iGCB culture. **h** Bar graph summarizing iPC differentiation normalized to WT B cells transduced with empty retroviruses (WT control). Data represents mean ± SD (n = 4, 3, 4, 3 biological replicates from left to right). **i** Immunoblot analysis of indicated proteins. **j**, **k** Day 4 iGCB cells of indicated genotypes were replated on fresh 40LB cells for plasma cell differentiation. Cells were harvested at indicated time points and analyzed by Immunoblot (**j**) and qRT-PCR (**k**) (n = 3 biological replicates). mRNA levels were normalized by Ct values of WT iGCB day 4 samples. Source data of (**h**, **k**) can be found in a Source Data file. Statistical analyses were performed using unpaired two-tailed Student's t-test.

decay through deadenylation, resulting in transient upregulation of c-Fos protein[6,45,62]. Five proteins, Csde1, poly(A) binding protein (PABP), PABP-interacting protein PAIP1, AU-rich element binding protein hnRNP D, and hnRNP R-like protein NSAP1, were identified to form a complex that brings the mCRD and poly(A) tail together, with Csde1 binding to the mCRD and PABP binding to the 3' poly(A) tail. Csde1 is able to bind both the mCRD sequence and PABP, thus establishing interaction between the poly(A)/PABP complex and the mCRD/Csde1 complex, which is associated with deadenylases (Fig. 10). Before the mCRD-containing mRNA is translated, this bridging complex may prevent deadenylation by stabilizing the poly(A)/PABP complex, thus blocking poly(A) nuclease access to the poly(A) tail. During translation, ribosomal transit across mCRD may displace or reorganize the bridging complex, expose the poly(A) tail to nuclease attack, leading to deadenylation and subsequent mRNA decay. The transient upregulation of Bach2 protein at the early stage of plasma cell differentiation is similar to transient expression of ERGs when cells transit from G0 into cell cycle. During germinal center response, rapid induction of Bach2 is essential for promoting GCB and memory B cell fates, while its downregulation is critical for plasma cell differentiation. During cellular proliferation, rapid induction of c-Myc is crucial for cell cycle progression, while sustained c-Myc expression would lead to oncogenic transformation[76]. In both scenarios, coupling mRNA translation and decay is highly suitable for and plays critical roles in coordinating those highly dynamic cellular processes. It is conceivable that target mRNAs of Csde1 and Strap regulated by this mechanism are not limited to Bach2, as many of them harbor Csde1 and Strap binding sites in their CDS regions and undergo active translation in response to B cell stimulation signals. Future investigations are warranted to identify other functionally important targets genes regulated by Strap and Csde1 through mCRD-mediated mRNA decay mechanisms, as well as additional RBPs contributing to those regulatory mechanisms.

This study illustrates the functional importance of collaboration between RBPs. Csde1 and Strap are RBPs with versatile functions. They are involved in many protein complexes and function in a broad spectrum of cellular processes[77]. In this study, Strap and Csde1 form a tight protein complex. This serves multiple purposes. Firstly, the Csde1-Strap complex stabilizes Csde1 protein. In the absence of Strap, the Csde1 protein level is drastically decreased (Fig. 7j). Secondly, Strap and Csde1 cooperate to achieve optimal binding to their common target mRNAs (Fig. 9e). Many RBPs, especially core RBPs expressed in a broad spectrum of cell types, exhibit neither specific nor high-affinity binding for the purpose of transient associations with RNA. The assembly of RNP complexes containing multiple RBPs would stabilize each RBP subunit, as well as enhance their specificity and affinity/avidity for RNA[78,79]. Thirdly, functions exerted by the Csde1-Strap complex are B cell-specific, as Csde1 and Strap could play their own roles in the absence of the other. Strap itself regulates mRNA splicing in embryonic stem cells[80] and cooperates with the SMN complex to control snRNP biogenesis[47], while Csde1 promotes cap-independent mRNA translation initiation via IRES elements[59]. As the RBP compendium of cells can vary prominently, it is conceivable that cell type-specific RBP complexes control target mRNAs in a cell-type-specific manner. It is also conceivable that certain proteins lacking well-defined RNA-binding domains but harboring intrinsically disordered regions are able to gain RNA-binding ability by associating with RBPs. Strap is one of such proteins. It is not a RBP in many cell types and does not have well-defined RNA-binding domains. In B cells, the Csde1-Strap interaction likely facilitates the transition of its disordered regions into ordered regions to gain RNA-binding ability[81]. Future investigations of cell type-specific functions and molecular mechanisms of action of RBPs will shed light on the complexity and functional importance of their regulation of gene expression under health and disease.

Methods

Mice

C57BL/6 J, *Rosa26-Cas9 (Cas9)* (Jax Stock 024858), and *Cγ1*-Cre (Jax Stock 010611) mice were purchased from the Jackson Laboratory and maintained in Xiamen University Laboratory Animal Center. *Csde1*$^{fl/fl}$ (stock number CKOCMP-01931-Csde1) and *Strap*$^{fl/fl}$(stock number T009705) mice were purchased from Cyagen and GemPharmatech, respectively. All these stains are on the C57BL/6 genetic background. All animal experiments were approved by Animal Care and Use Committee of Xiamen University (XMULAC20170323). All mice were housed in a specific pathogen-free (SPF) facility under a 12 h light-dark cycle at the Xiamen University Laboratory Animal Center. The light time was from 8 a.m. to 8 p.m., and the room temperature was kept at 22–24 °C and humidity at 50–70%. Both male and female mice (8–10 weeks old) were used in this study unless stated otherwise. The control and experimental mice utilized in all mouse experiments described in this paper were co-housed and were euthanized by a carbon dioxide method.

Plasmids

The sgRNA sequences were designed and cloned into the MSCV-U6-sgRNA-Pgk-Puro-T2A-BFP plasmid (addgene, plasmid #86457) by T4 DNA ligation. All sgRNA sequences used in this study are listed in Supplementary Table 1. For ectopic expression of protein-coding genes, Strap, Csde1, Bach2, and Atp2a2 cDNAs were PCR-amplified from mouse cDNA. To enhance expression efficiency of some large proteins, we cloned the Ef1a promoter into the RV-IRES-GFP and RV-IRES-mCherry retroviral vectors to generate the RV-Ef1a-IRES-GFP and RV-EF1a-IRES-mCherry vectors with ligation-independent cloning. Strap and Bach2 cDNAs were cloned into RV-IRES-GFP, while Csde1 and Atp2a2 cDNAs were cloned into RV-Ef1a-IRES-GFP and RV-EF1a-IRES-mCherry vectors, respectively. To construct Csde1 truncation mutant (Csde1 Δc), nucleotide 1-2211 of Csde1 coding region was amplified and

https://doi.org/10.1038/s41467-025-58212-8

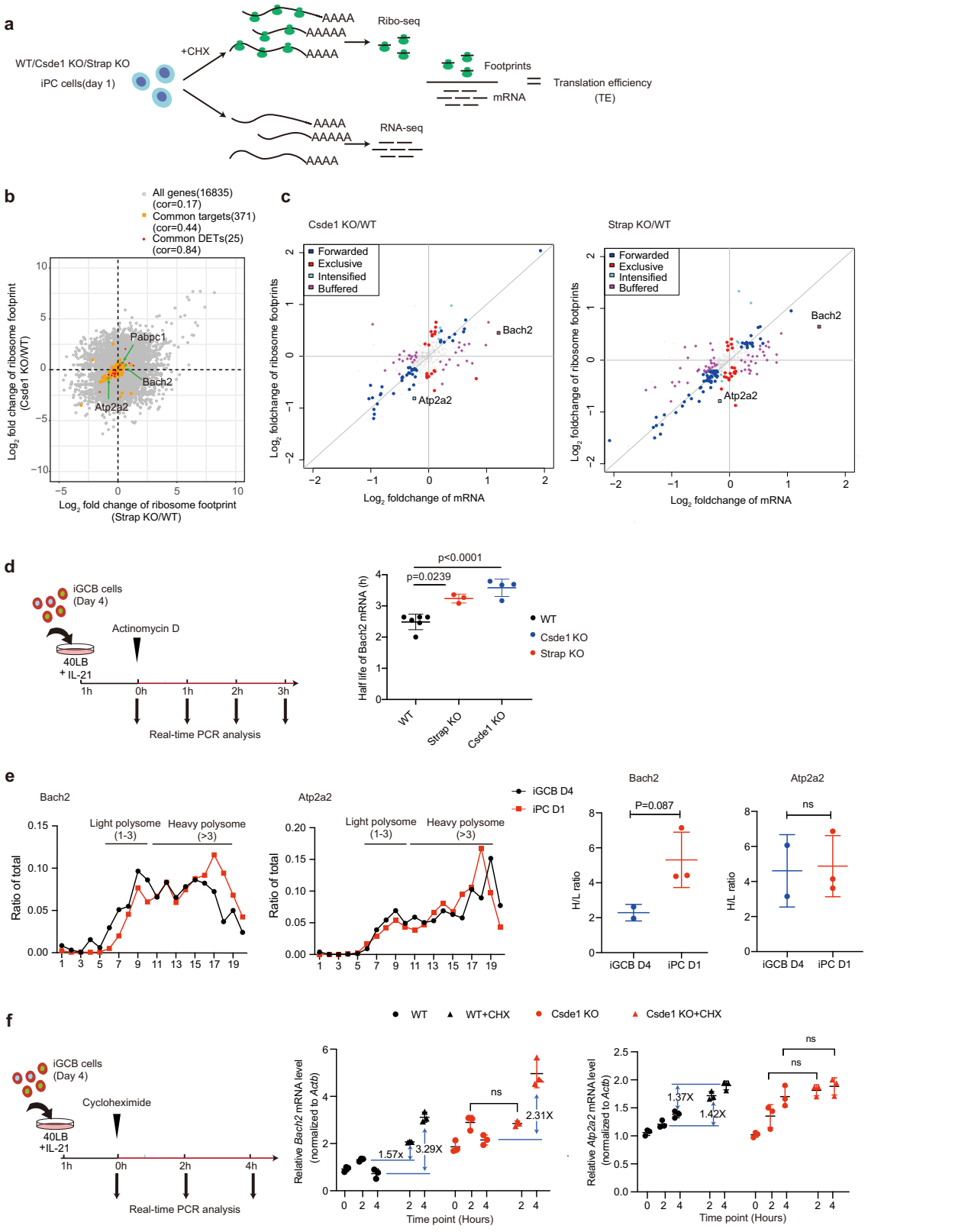

cloned into the RV-Ef1a-IRES-GFP vector. The Csde1-Strap fusion plasmid (Csde1 Δc-Strap) was constructed by inserting a short linker peptide (-GGGSGGGSGGGS-) and the full-length Strap coding sequence into RV-Ef1a-Csde1 Δc -IRES-GFP plasmid, right before the stop codon of Csde1 Δc. All the constructs were confirmed by Sanger sequencing.

Cell lines

HEK293T cells were a gift from Jiahuai Han lab (Xiamen University) and maintained in DMEM (Gibco) complete medium with 10% FBS, 100 U/mL penicillin, and 100 U/mL streptomycin (Gibco). NIH3T3 derived 40LB feeder cells expressing CD40L and BAFF were maintained in DMEM complete medium[19].

Fig. 8 | Strap and Csde1 regulate target mRNA translation and stability. **a** Schematic representation of Ribo-seq and RNA-Seq experiments. **b** Scatter plot showing correlation of ribosome footprint changes caused by deletion of Strap or Csde1. Gray, all genes; orange, common targets of Strap and Csde; red, common DETs identified in Fig. 6e. cor, correlation. **c** Scatter plots showing log2 fold changes in ribosome footprints and RNA expression levels of common targets in Csde1 or Strap KO cells at iPC day 1. **d** The *Bach2* mRNA stability was assessed by qRT-PCR in iGCB day 4 cells freshly re-plated on 40LB cells in the presence of IL-21 and treated with Actinomycin D. Left, experimental outline. Right, half-life of *Bach2* mRNA in iGCB cells from WT ($n = 6$), Strap cKO ($n = 3$), Csde1 cKO ($n = 4$) mice. Each symbol represents one independent experiment with three technical replicates. See also Supplementary Fig. 15d for one representative experimental result of mRNA decay. **e** Representative result of *Atp2a2* and *Bach2* mRNA distribution in the sucrose gradient of iGCB day 4 and iPC day1 cells. Ratio is the mean value of three technical replicates. The ratios of *Bach2* and *Atp2a2* mRNA distribution in heavy (ribosome>3) and light polysome (ribosome < =3) area of iGCB day 4 ($n = 2$) and iPC day1 ($n = 3$) B cells were analyzed statistically. **f** *Bach2* and *Atp2a2* mRNA expression was quantified in cycloheximide-treated iGCB cells co-cultured with 40LB cells in the presence of IL-21 following the experimental outline. Representative results of qRT-PCR analysis of *Bach2* and *Atp2a2* mRNA levels. The fold changes between cycloheximide (CHX)-treated and control samples at indicated time points were shown. $n = 3$ biological independent replicates. Data represents mean ± SD. Statistical analyses were performed using unpaired two-tailed Student's test (ns, not significant). Source data of (**d**–**f**) is provided in a Source Data file.

In vitro plasma cell differentiation

Naïve B cells were purified from mouse splenocytes by negative selection with biotin-conjugated antibodies against CD5, CD9, CD43, CD93, and Ter119. Following the previously reported protocol[82], naïve B cells were cultured in 6- or 12-well plates in the presence of 40LB cells irradiated with 120 Gy X-ray. The medium was supplemented with 10% FCS, 5.5×10^{-5} M *β-mercaptoethanol* (2-ME), 10 mM HEPES, 1 mM sodium pyruvate, 100 U/mL penicillin, and 100 μg/mL streptomycin (GIBCO), 1× NEAA (Gibco). Naïve B cells were cultured with 40LB cells in the presence of IL-4 (Novoprotein, CK74) for 4 days to differentiate into iGCB cells. On day 4, iGCB cells were re-plated with fresh 40LB cells in the presence of 10 ng/mL IL-21 (Novoprotein, CK10). After another 4 days of culture, cells were harvested for flow cytometry analysis.

Retroviral transduction

For virus production, HEK293T cells were plated in 6-well plates one day before iGCB culture. On the same day when naïve B cells were plated for iGCB culture, HEK293T cell culture medium was replaced with fresh medium when cells reached ~80% confluency. 1–2 h following medium replacement, each well was transfected with 3 ug retroviral plasmid and 1 ug packaging plasmid (pCl-Eco, addgene#12371) by the calcium phosphate method. Medium was replaced with fresh one at 6–8 h after transfection. For plasmids encoding large proteins, 2.5 mM sodium butyrate (Sigma) was added to promote virus production. Retroviral supernatants were collected at 48–72 h after transfection and cell debris was removed by centrifugation. For retroviral transduction, naïve B cells were cultured in the iGCB system as described above. On day 2.5 of iGCB culture, 8 mL medium from each well of 6-well plates was collected and kept in 37 °C water bath. The remaining medium was replaced with 1 ml fresh iGCB medium supplemented with polybrene (Sigma, TR-1003-G) and IL-4 (Noveprotein, CK74) to a final concentration 5 ng/mL and 1 ng/mL, respectively. 1 mL retroviral supernatant was added to each well, followed by spinoculation at 2500 rpm for 60 min at 32 °C and incubation at 37 °C for 4–6 h before previously collected medium was added back to wells.

RNA interactome capture

The experiments were performed following the previously published protocol[18]. 4SU (Sigma) was added to iGCB culture at a final concentration of 100 μM 16 h before harvesting iGCB day 4 cells. 1×10^8 iGCB cells were crosslinked with 0.15 J/cm^2 365 nm UV light and treated with lysis buffer to completely lyse cells in 50 ml Falcon tube before storing at −80 °C until further processing. Since naïve B cells were purified ex vivo while iPC cells were sensitive to toxicity of 4SU, 4SU treatment was not applied to those cells. 3×10^8 naïve B or 0.8×10^8 iPC cells were harvested, crosslinked with 0.15 J/cm^2 254 nm UV light, and lysed in the same way as iGCB cells. In parallel, equal numbers of naïve B, iGCB, and iPC cells were lysed without UV crosslinking and used as non-crosslinked controls. For RNA interactome capture, frozen cell lysates were thoroughly thawed and mixed with pre-equilibrated oligo(dT)$_{25}$ beads (ThermoFisher, Cat. 61006) at room temperature for 2 h with gentle rotation. Subsequently, beads were pelleted by magnets, and supernatants were transferred to new tubes for next round of capture. Beads were washed in 35 ml ice cold lysis buffer with gentle rotation for 5 min at 4 °C and pelleted by magnets. Supernatant was removed. Beads were sequentially washed with ice-cold buffer I, II, and III (twice for each buffer) containing decreasing amounts of salt and detergent. Beads were transferred to microcentrifuge tubes, followed by addition of 500 μl elution buffer and incubation at 55 °C for 3 min to elute RNA-protein conjugates. The above RNA capture steps were repeated for two more rounds. All eluates were pooled with a final volume of ~1.2 ml. RNA in the eluate was digested by adding 10× RNase buffer, 200 U RNase T1 (Sigma, cat. R1003), and RNase A (Takara). After RNase-treatment, eluate was transferred to an Amicon Ultra-10 3 kDa cutoff device for protein concentration. The protein samples were now ready for silver staining and mass spectrometry analyses.

Protein sample preparation for mass spectrometry analysis

The above prepared protein samples were processed with gel-aided sample preparation (GASP) for mass spectrometry analysis. Briefly, 50 μL samples were prepared in the presence of 10 mM TCEP to reduce disulfide bonds. Subsequently, reduced cysteines were alkylated with 10 mM iodoacetamide, and an equal volume of 30% Acrylamide/bis-acrylamide solution was added. The mixture was then polymerized with 2 μL of TEMED and 2 μL of 10% ammonium persulfate, and the gel was left at room temperature for 20 min until it solidified. The solidified gel was cut into small pieces and fixed by adding 1 mL of methanol/acetic acid/water (50/40/10) for 10 min in an overhead mixer. After pulse centrifugation, the supernatant was discarded, and the gel pieces were washed with 1 mL of 100 mM NH_4HCO_3 for 10 min in a rotator. To dehydrate the gel pieces and remove the supernatant, 1 mL of acetonitrile was added. In most cases, three NH_4HCO_3/ACN wash cycles were performed. After discarding the supernatant, the gel pieces were dried by adding 500 μL of acetonitrile until they agglomerated at the bottom of the tube. Next, 100 μL of trypsin solution (20 μg/μL) was added to the dry gel pieces for proteolysis at 37 °C overnight.

The subsequent peptide extraction process involved adding 100 mL of extraction buffer (1:2(vol/vol) 5% formic acid/acetonitrile) to each tube, followed by incubation for 15 min at 37 °C in a shaker. Peptide extraction was facilitated by adding 200 μL of acetonitrile. The supernatant was transferred into a new tube, and the gel pieces were rehydrated in 5% formic acid, followed by dehydration with 200 μL of acetonitrile. Supernatants were combined after further dehydration in 50 μL of acetonitrile. Finally, the samples were dried in a vacuum concentrator and resuspended in 0.1% FA for LC-MS analysis.

LC-MS/MS analysis

Peptides were analyzed using an ultra HPLC EASY-nL-LC 1000 coupled with an online Orbitrap Fusion mass spectrometer (Thermo Scientific, CA, USA). Mobile phase A consisted of 0.1%

https://doi.org/10.1038/s41467-025-58212-8

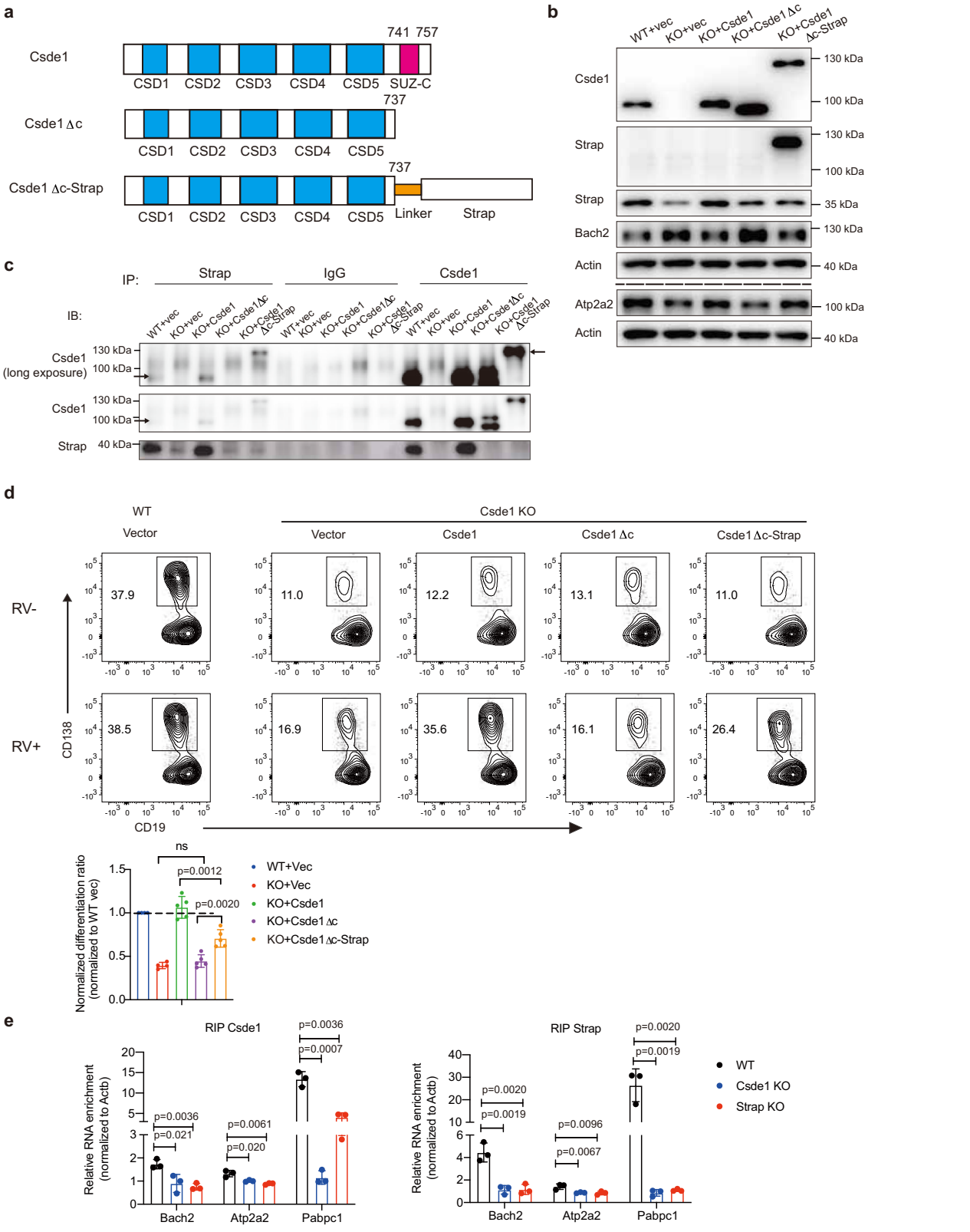

formic acid (FA), 2% acetonitrile (ACN), and 98% H2O, while mobile phase B consisted of 0.1% FA, 2% H2O, and 98% ACN. Samples were directly loaded onto a 100 µm I.D. 150 mm analytical column (in-house packed with 1.9 µm C18 resin, Dr. Maisch, Germany). A 120-min gradient (phase B: 3–8% in 8 min, 8–20% in 85 min, 20–40% in 17 min, 40–95% in 5 min, 95–95% in 5 min) was used at a static flow rate of 300 nL/min. The MS data were acquired in a data-dependent mode. For MS1, the Orbitrap was used to acquire the data, with a scan range of 300 to 1800 m/z at a resolution of 120,000, and the AGC target set at 5×10^5. Precursor ions with 2–8 charges were selected for tandem MS analysis. For MS2, the scan range was 100 to 1800 m/z in the ion trap, with the AGC target set at 1×10^4, and a maximum injection time of 200 ms.

Fig. 9 | The Strap-Csde1 interaction is essential for target mRNA binding and plasma cell differentiation. a Schematic representation of domain structure of Csde1 and mutants. Csde1 Δc, C-terminal truncated. Csde1 Δc-Strap, C-terminal truncated with Strap tethered to its C-terminus through a flexible glycine-serine linker. **b** Immunoblot analysis of indicated proteins in WT and Csde1 KO B cells transduced with retroviruses encoding Csde1 and mutants. Atp2a2 expression was examined in a separate gel. **c** Immunoblot analysis of proteins immunoprecipitated by indicated antibodies from WT and Csde1 KO B cells transduced with retroviruses encoding Csde1 and mutants. The arrows on the left indicate Csde1, while the arrow on the right indicates Csde1 Δc-Strap. **d** Representative FACS plots of iPC differentiation of WT and Csde1 KO B cells transduced with retroviruses encoding Csde1 and mutants. The bar graph summarizes iPC differentiation ratio normalized to WT B cells transduced with empty retroviruses (WT+Vec). $n = 4,4,5,5,6$ biological replicates from left to right. **e** Representative results of qRT-PCR analysis of indicated mRNAs pulled down by Csde1 or Strap antibodies from WT, Strap KO, and Csde1 KO B cells from 3 independent experiments with 3 technique replicates in each experiment. Data represent mean ± SD. Statistical analyses were performed using unpaired two-tailed Student's test. Source data of (**d**, **e**) is provided in a Source Data file.

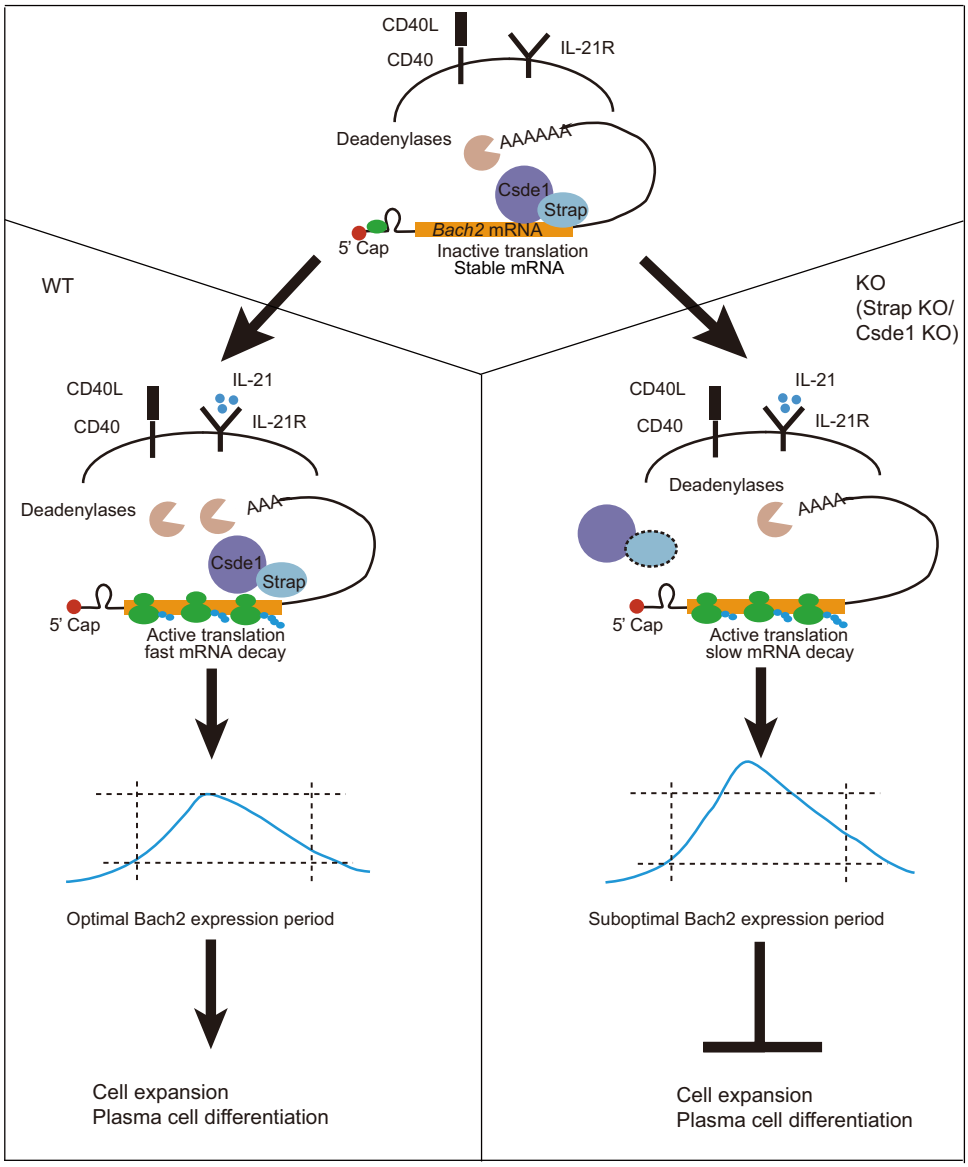

Fig. 10 | A Csde1-Strap complex regulates plasma cell differentiation by coupling the translation and decay of Bach2 mRNA. In the absence of IL-21 stimulation, *Bach2* mRNA translation and decay occur at low levels, probably due to the presence of complex secondary structures in the 5'UTR of *Bach2* mRNA. The Csde1-Strap complex bridges the poly(A) tail and coding region of *Bach2* mRNA, and prevents deadenylation. Upon IL-21 and CD40L stimulation, translation of *Bach2* mRNA is significantly upregulated, leading to reorganization of the bridging complex when ribosome transits through the coding region, exposure of the poly(A) tail to deadenylases, and subsequent mRNA decay. In the absence of Csde1 or Strap, the bridging complex is not able to form, leading to decoupling of translation and decay of *Bach2* mRNA and elevated Bach2 protein expression, which impairs B cell expansion and plasma cell differentiation.

RNA interactome data analysis

This data was analyzed mainly following the protocol described by Castello et al.[18]. LC-MS/MS raw spectra were processed using MaxQuant software (version 1.5.3.30) to extract ion count measures for each peptide. The UniProt mouse protein sequence database containing 50,961 sequence entries (download date: April 05, 2017) was used for database search. The ion counts were processed using Perseus[83] software for filtering, imputation, Z-score normalization following the manufacturer's instructions. After calculating the ratios between crosslinked groups and non-crosslinked groups, a one-

sample t-test was performed to analyze the significantly enriched proteins.

CRISPR/Cas9-mediated screening

Cas9-GFP B cells were cultured with 40LB cells in 6-well plates. At day 2.25, cells were transduced with retroviruses encoding BFP and the custom-made mouse RBP sgRNA library at an MOI of 0.2. One day later, 5 ml iGCB medium in each well of the 6-well plates was replaced with same volume fresh medium supplemented with 0.5ug/ul puromycin. Two days later, transduced cells were collected and replated for next stage of culture. A portion of them was sorted and saved as the "input" sample of the screen. At day 4 of the 2nd stage of culture, $BFP^+GFP^+CD138^-$ and $BFP^+GFP^+CD138^+$ B cells were sorted and saved as the "CD138-" and "CD138 + " samples of the screen, respectively. A portion of BFP^+GFP^+ cells was sorted and saved as the "total B cells" sample of the screen. Sorted cells were snap-frozen in liquid nitrogen in 1.5 ml microtubes and stored at −80 °C for future analysis. At least 2.5 million cells were sorted for each sample to ensure greater than 500 x coverage for the sgRNA library.

NGS library generation, sequencing, and data analysis

Genomic DNA (gDNA) was extracted with the MicroElute Genomic DNA Kit (Omega, cat. D3096-02). The genomic regions targeted by sgRNA were amplified to prepare sgRNA library for NGS as described in a published protocol[31]. To prepare the sgRNA library for NGS, set up a reaction for each of the 10 NGS-Lib-Fwd primers and 1 NGS-Lib-Rev to amplify as much as genomic DNA as possible in each sample. Barcoded NGS-Lib-Rev primers enable sequencing of samples from different screening conditions and bioreps. After the PCR reactions of each sample were complete, the reactions were pooled and PCR products were purified using a Zymo-Spin V with Reservoir following the manufacturer's protocol. The purified products were ~260–270 bp size-selected on a DNA agarose gel to remove PCR artifacts and excessive primers. The size-selected PCR products were purified again using the universal DNA purification kit (TIANGEN, Cat. DP214-03). The purified PCR products were quantified by Qubit fluorometer and samples with unique barcodes were pooled in equal amounts. The pooled libraries were then sent for NGS. A coverage of >500 reads per sgRNA in each library was required. For sequencing data analysis, sgRNA counts were calculated with count_spacers.py, a Python script provided in the protocol[31]. The sgRNA count tables of all sgRNA libraries, including input, total B cells, $CD138^+$, and $CD138^-$, were used as inputs for the Mageck software[34] to determine gene-level LFC and rank for the expansion (total B cells vs input) and differentiation ($CD138^+$ vs total B cells) screens. A list of control sgRNAs (sgNTC) was included in the custom-made mouse RBP sgRNA library for normalization and for generating the null distribution of RRA. Paired sample comparisons and "mean" normalization method were used for data analysis. The Alphamean method, which only considered median/mean sgRNAs that are ranked in front of the alpha cutoff in RRA, was used to calculate gene LFC for the differentiation screen. Our statistical cutoff for gene level enrichment was set at p-value less than 0.01, absolute LFC at more than 0.5 for the expansion screen, and more than 0.3 for differentiation screen.

RNA-seq

iGCB cells from Cas9-GFP transgenic mice were transduced by retroviruses encoding sgStrap, sgCsde1, sgPrdm1, and sgNTC to generate B cells lacking indicated genes. Transduced cells were sorted on iGCB day 4 and iPC day 1, 2, and 4. Total RNA was extracted using RNAeasy Kit (QIAGEN) following the manufacturer's instructions. RNA samples were sent to Novogene for sequencing. The clean data, with adapter sequences trimmed and low-quality reads removed, was used for downstream analysis. The clean data was processed to read counts following the Hisat2-StringTie pipeline[84]. Using prepDE.py provided by StringTie, read count information was extracted for differential analysis conducted by DESeq2[85]. PCA analysis was performed using the embedded function in DESeq2. GO enrichment analysis of differential expression genes was performed in Metascape[86].

Immunization

Antigens for immunization were prepared by mixing NP_{20}-OVA (Biosearch Technologies) dissolved in PBS and 10% $KAl(SO_4)_2$ at a 1:1 ratio, in the presence or absence of LPS (Sigma, Escherichia coli 055:B5), and adjusting pH to 7 to form precipitate. 50 μg NP-OVA and 10 μg LPS precipitated together with alum was injected intraperitoneally (i.p.) into each mouse. 14 days after immunization, NP-specific ASCs were measured by ELISpot assay. NP-specific GCB and PC cells were examined by flow cytometry. 50 μg NP-OVA precipitated in alum was injected i.p. into each mouse for NP-specific antibody responses. Serum samples were collected at day 0, 7, 14, 21 and analyzed by ELISA to determine the concentrations of NP-specific antibodies.

Flow cytometry

Single cell suspensions prepared from the spleen were stained with surface markers in FACS buffer (PBS with 0.5% BSA) at 4 °C for 20–30 min, washed, and resuspended in FACS buffer. For NP staining, single cells were incubated with 4-Hydroxy-3-nitrophenylacetyl hapten conjugated to PE protein at a ratio 1:5000 for 1 h at 4 °C, then stained with other surface markers as mentioned above. For IgG1 staining, cells were fixed with Fixation/Permeabilization solution (BD, cat. 554722) at 4 °C for 1 h after surface marker staining, washed, and stained with anti-mouse IgG1 in 1x Perm/Wash buffer. The surface marker antibodies included: CD19, CD138, CD45.1, CD3, B220, Fas, GL7, IgD, NP, IgG1, CD43, BP-1, IgD, IgM, CD93, CD25, CD21, CD23, CD24 (Supplementary Table 19). All flow cytometry data were acquired on Fortessa or Fortessa X20 flow cytometers (BD) and analyzed using the FlowJo software (Treestar, Inc.).

ELISPOT. NP-specific IgG1 splenic ASCs following immunization with 50 μg NP-OVA and 10 μg LPS precipitated in alum were measured by ELISpot assay on a MultiScreen 96-well filtration plate (Millipore, MSIPS4W10) coated with 10 μg/ml NP_{29}-BSA. Cells were serially diluted and added to individual wells in triplicates, followed by incubation for 3 h at 37 °C with 5% CO_2. Anti-NP IgG1 spots were detected by biotin-conjugated anti-mouse IgG1 antibody (Southern Biotechnology, 1070-08) in combination with Av-HRP and AEC substrate (Vector Laboratories, A-2004& SK-4200).

ELISA. Microplates (ThermoFisher, 439454) were coated with 10 μg/mL NP_{29}- or NP_7-BSA to capture total and high affinity NP-specific antibodies, respectively. Nonspecific binding was blocked with 0.5% BSA in PBS (PBSA). Serum samples were serially diluted in PBSA and incubated in blocked plates at room temperature for 2 h. Plates were incubated with biotin-conjugated anti-IgM (1020-08, Southern Biotech) or anti-IgG1 (1070-08, Southern Biotech) for 1 h at 37 °C and with streptavidin-alkaline phosphatase (Roche) at RT for 1 h, followed by incubation with alkaline phosphatase substrate solution containing 4-nitro-phenyl phosphate (Sigma N2765) for color development. Plates were quantified on a Tecan Spark multimode reader.

RNA imaging

RNA imaging was performed following the online biotin-based labeling protocol (https://www.protocols.io/view/biotin-labeling-of-immunoprecipitated-na-v1pre-7z4hp8w)[87]. In brief, iPC day 2 cells were collected and crosslinked as required for eCLIP experiments. All the procedure was performed at room temperature before cell lysis. Cell lysates of the UV crosslinked cells were treated with Turbo DNase (Thermo) and RNase I (Ambion, 50U for high [++] and 4U for low [+] dilution). Next, 20 μL

Dynabeads Protein G (Thermo) conjugated with 1 µg Csde1 antibody (Abcam, cat. ab201688) were added to the lysates, followed by overnight rotation. For Strap, 20 µL of Dynabeads Protein A (Thermo) conjugated with 2 µg antibody (Bethyl, cat. A304-735A) were used. After rotation overnight, samples were washed three times with high-salt wash buffer followed by two washes with no salt buffer. FastAP and T4PNK reactions were performed on bead as previously described in protocol, followed by two washes with high-salt buffer and two washes with no salt buffer. A modified RNA linker ligation was performed using 500 pmol pCp-Biotin (Jena Bioscience). Afterward, samples were incubated at 16 °C and mixed at 1600 RPM (30 s on; 30 s off) for 3 h. After ligation, samples were washed twice with high-salt wash buffer and twice with no salt buffer, followed by standard SDS-PAGE electrophoresis and transferred to nitrocellulose membranes. Visualization was performed using the Chemiluminescent Nucleic Acid Detection Module Kit (Thermo) following the manufacturer's instructions for blocking, washing, and labeling. Imaging was performed on the Amersham Imager 600 (GE Healthcare).

Enhanced crosslinking and immunoprecipitation (eCLIP)

$2.5–3 \times 10^7$ iPC day 2 cells were prepared for this experiment following negative selection to remove 40LB cells. Enhanced crosslinking and immunoprecipitation sequencing (eCLIP) experiments were performed following manufacturer's instructions (Eclipse Bioinnovations Inc., https://eclipsebio.com/services-kits/rbp-eclip/). Briefly, purified iPC cells were UV-crosslinked, followed by cell lysis and treatment of cell lysates with RNase I (4U, Ambion) to digest RNA. The Csde1 or Strap protein-RNA complexes were immunoprecipitated with antibodies described in RNA imaging. An RNA adapter was ligated to the 3′ end of RBP-bound RNA fragments. Proteinase K was added to digest proteins before reverse transcription of RNA. cDNA was ligated to the 3′ end of single-stranded DNA adapters that serve as unique identifiers for PCR duplicates. Finally, the paired-end cDNA fragments were amplified and sent to Azenta Life Sciences for sequencing.

eCLIP data analysis

eCLIP data were analyzed using the data analysis pipeline V2.0 provided in ENCODE projects (https://www.encodeproject.org/pipelines/ENCPL357ADL/). Only read1 of sequencing data was used for the following analysis. Since sequencing reads had been demultiplexed by providers, we started with trimming reads using Cutadapt (version 2.2). The trimmed sequences were then processed in UMI-tools[88] to extract umi sequences in reads. Reads were mapped to the mouse RepBase to remove repetitive elements using STAR version 2.5.2b. The outputs from STAR rmRep can be counted as the number of reads mapping to each repetitive element with Samtools view and count_aligned_from_sam. The unmapped reads from the above STAR alignment were mapped to mm10 using STAR. The output bam files were removed of duplicates of PCR with dedup command provided by UMI-tools. Then custom scripts, sortSam, in gatk from yeo lab were used to sort resulting bam files for use downstream. Clipper provided by the Gene Yeo lab was then used for peak calling from output bam files generated from IP samples following the usage in GitHub. The script named merge_peaks in the second eCLIP-seq processing pipeline was used to discover RBP binding sites through normalization against the input control. Finally, merged_peaks_bed files were generated, which contain binding sites as determined by entropy-ordered peaks between two replicates. Since the enrichment criteria set by the script are too stringent, we decreased the log2foldchange required for peak signals from 3 to 2 to generate more peaks for subsequent analyses. Tracks were visualized using the Integrative Genomics Viewer (IGV). The peaks in merged_peaks_bed files were annotated and used for metagene plots by online analysis provided by RNAmod website[89] (http://61.147.117.195/RNAmod/index.php).

TMT labeling, LC-MS/MS, and data analysis

iPC day1 cells differentiated in vitro from WT, Csde1 cKO, and Strap cKO mice were FACS sorted and snap frozen in liquid nitrogen. EasyPep kit (ThermoFisher, A45733) was used to for TMT labeling following the manufacturer's instructions. For LC-MS/MS analysis, samples were acquired using an Orbitrap Eclipse mass spectrometer in line with a Vanquish Neo UPLC system. For data analysis, all acquired data were searched and quantified utilizing the Thermo Proteome Discoverer (2.5.0.400 version). Full MS and MS/MS spectra were searched against the *Mus musculus* database downloaded from Uniprot (www.uniprot.org). The differential expression analysis was performed with Perseus[83] software to determine log2foldchange of proteins between KO and WT cells, *p*-values, and *q*-values.

Immunoblot and immunoprecipitation

For immunoblot, cells pellets were lysed in lysis buffer (20 mM Tris-Hcl PH 7.5, 1% Triton-X-100, 1 mM EGTA, 1 mM EDTA, 1 mM Na_3VO_4, 150 mM NaCl, 2.5 mM Napip and 1 mM β-glycerophosphate) supplemented with protease inhibitors, SDS loading buffer and 2.5% β-ME at 4 °C. After incubation at 95 °C for 5 min, supernatants were briefly centrifuged, collected, resolved on SDS-PAGE gels, and transferred to PVDF membrane (Millipore, IPVH00010). The membrane was incubated overnight at 4 °C with primary antibodies diluted in 1× Tris-buffered saline (TBS) (10 mM Tris-HCl, pH 8.0, and 150 mM NaCl) with 5% (wt/vol) bovine serum albumin (BSA) or nonfat milk, washed 3 times in TBS buffer with 0.5% Tween 20, and incubated with horseradish peroxidase (HRP)-conjugated goat anti-rabbit or goat anti-mouse antibodies in TBS at room temperature for 1 h. The membrane was then washed 3 times in TBS buffer with 0.5% Tween 20. Protein bands were visualized with ECL Select Western Blotting Detection Reagent (GE Healthcare) following the manufacturer's instructions (GE Healthcare). Images were acquired with Amersham Imager 600 (GE Healthcare).

For immunoprecipitations, $2–4 \times 10^6$ iPC cells following negative selection to remove 40LB cells were lysed on ice for 30 min in lysis buffer supplied with protease inhibitors. Following centrifugation, supernatant was transferred to a new tube and incubated with Strap or Csde1 antibody, or rabbit IgG control (Sigma#I5381) for 4 h at 4 °C. The antibody and lysate slurry were incubated with Protein A/G magnetic beads (Bimake cat. B23202) overnight. Samples were then washed with lysis buffer for 5 times and eluted with lysis buffer used in the immunoblot procedure through denaturing at 95 °C for 5 mins. All antibodies were listed in Supplementary Table 2.

Ribosome profiling

iPC day1 cells were used for Ribo-seq analysis. Cells were treated with cycloheximide (CST Cat. 2112S) at a final concentration of 100 µg/mL, and sorted to collect live iPC cells and to remove 40LB cells. After sorting, each sample should contain more than 2×10^6 cells. Sorted cells were snap frozen in liquid nitrogen and stored at at −80 °C until further processing. For ribosome profiling, cell samples were processed as described in the protocol[90]. Firstly, samples were lysed in lysis buffer. Lysates were centrifuged at 20,000 × *g* for 10 min at 4 °C. Supernatant was collected. 10 µL RNase I (NEB, Ipswich, USA, M0307) and 6 µL DNase I (NEB, Ipswich, USA, M0303) were added to 400 µL of lysate, followed by incubation for 45 min at room temperature with gentle mixing. Nuclease digestion was stopped by adding 10 µL SUPERase·In RNase inhibitor (Ambion, TX, USA, AM2696). Size exclusion columns (Illustra MicroSpin S-400 HR Columns, GE Healthcare, 27-5140-01) were equilibrated with 3 mL of polysome buffer by gravity flow and centrifuged at 600 × *g* for 4 min at room temperature. The digested products from last step were added to the pre-equilibrated columns, which were centrifuged at 600 × *g* for 2 min. 10 µL of 10% (wt/vol) SDS were then added and RFs with size greater than 17 nt were isolated using the RNA Clean and Concentrator-25 kit (Zymo Research,

Irvine, USA, R1017). rRNA was removed using the method reported previously[91]. In brief, short (50–80 bases) antisense DNA probes complementary to rRNA sequences were added to solution containing RFs. RNase H (NEB, Ipswich, USA, H0110) and DNase I were added to digest rRNA and residual DNA probes. Finally, RFs were further purified using magnet beads (Vazyme, Nanjing, China, N412). After obtaining RFs, Ribo-seq libraries were constructed using NEB Next® Multiple Small RNA Library Prep Set for Illumina® (E7300S, E7300L). Briefly, adapters were added to both ends of RFs, followed by reverse transcription and PCR amplification. PCR products in the 140–160 bp size range were enriched to generate a cDNA library and sequenced using Illumina HiSeq by Gene Denovo Biotechnology Co. (Guangzhou, China).

Ribosome profiling data analysis

Ribosome profiling data was analyzed following the workflow described in RiboCode[92] software. Adapters, low-quality reads, and reads aligned to rRNA were removed from the raw data. The remaining reads were aligned to genome using STAR[93] and output bam files were used for the following analyses. With the scripts provided by RiboCode, the length range of RPF reads and translated ORFs was determined. Ribosome profiling data were integrated with matched RNA-seq data to reveal translational regulation. RNA-seq data obtained from the same samples were processed to read counts as described in the RNA-Seq session. Using ModifyHTseq script provided by RiboMiner[94] software, read counts of ribosome footprints were generated. DeltaTE package analysis was performed to integrate Ribo-seq and RNA-seq data to analyze genome-wide translational regulation[70].

Polysome profiling

iPC day 1 cells were analyzed by polysome profiling following the protocol described in a previously published paper[95]. In brief, 2×10^7 iPC day 1 cells were collected and treated with cycloheximide (CST, Cat. 2112S). Treated cells were washed once in 10 ml hypotonic buffer, and cytosolic fractions were extracted with a total 600ul of 1:1 mix of hypotonic buffer and hypotonic lysis buffer. After 20 min of incubation on ice, nuclei were removed by centrifugation at $2300 \times g$ for 10 min. Supernatant was centrifuged on a 15–45% (w/w) of RNase inhibitor-containing sucrose gradient at 40,000 rpm for 1.5 h using a Beckman SW41 rotor. The resulting gradient was separated into 20 fractions using BR-188 Density Gradient Fractionation System (Brandel, Cat. BR-186-5). 1.5 µl 80 pg/ul exogenous RNA control (customed synthesized, full-length sequence: ACUUGCAAAGCCAAUUCCCGAAGAUCGUCUCAAUCGCACAGGAUCCCAAGCUUGAAUUCAUGUUAUAACACUUCUCUCAUGCCUGAAACUAAUGUCCUACUGUUCACUACAAUGG) was added to 100ul samples aliquoted from each fraction, followed by extracting total RNA with AG RNAex Pro reagent (Cat. AG21102) following manufacturer's instructions. Reverse transcription was performed with equal amounts of the RNA samples using ChamQ Universal SYBR qPCR Master Mix (Vazyme, Cat. Q711-03) following manufacturer's instructions. Indicated mRNA was amplified and measured by ChamQ Universal SYBR qPCR Master Mix (Vazyme, Cat. Q711-03). CT values were normalized to the spiked-in exogenous RNA control. Ratio of total in each fraction was calculated.

mRNA half-life measurement

Newly plated iGCB cells in iGCB medium supplemented with IL-21 were used for mRNA half-life measurement. After 1 h incubation with IL-21, cells were treated with 5ug/ml actinomycin D (ENZO, cat.BML- GR300) and harvested at 0, 1, 2, 3 h after treatment. Cell samples were treated with AG RNAex Pro reagent immediately after harvesting and total RNA was extracted. Equal amounts of RNA samples were used for reverse transcription and quantitative PCR. CT values of indicated mRNA were normalized to beta-actin mRNA. mRNA half-life was calculated as previously described[96].

RNA immunoprecipitation

RNA immunoprecipitation (RIP) was performed following the IP procedure of the eCLIP experiment[61]. At least 2×10^6 iPC cells were required for one sample. In brief, indicated antibody was coupled to Dynabeads Protein G or Protein A (Thermo) for 4–6 h at 4 °C. When the incubation of the antibody and beads was nearly completed, cell samples were lysed in ice-cold lysis buffer supplemented with Proteinase Inhibitor Cocktail(Thermo, Cat. 87786) and RNaseOUT(Invitrogen, Cat. 10777019), sonicated using Bioruptor plus (DIAGENODE), and centrifuged to remove nuclei. Supernatants were transferred to new tubes, followed by adding washed antibody-bead slurry and rotating overnight at 4 °C. Before adding the antibody-bead slurry, 30ul of each supernatant was removed and stored as input. After overnight incubation, beads were washed with high-salt buffer three times and wash buffer twice. Beads were now ready for Western blot and total RNA extraction. Half of the beads in 40 µL wash buffer was transferred to a new tube for total RNA extraction and qPCR quantification. The remaining half was added with loading buffer, Proteinase Inhibitor Cocktail, and reducing reagent (Thermo, Cat.NP0004), followed by denaturing in a Thermomixer at 1150 rpm, 65 °C for 10 min. Beads were removed and the remaining samples were analyzed by Western blot.

Statistics and reproducibility

All statistical analyses were completed using Prism 8 (GraphPad) or the R statistical language scripts and packages specified, with details of the individual statistical tests indicated in the figure legends. No statistical methods were used to estimate sample size or to include/exclude samples. Multiple sgRNAs were used to knockout a gene to exclude off-target effect. All experiments were performed at least twice (unless otherwise indicated in the figure legend).

Reporting summary

Further information on research design is available in the Nature Portfolio Reporting Summary linked to this article.

Data availability

Sequencing data generated in this study, including Ribo-seq, RNA-seq, pooled CRISPR screening, and eCLIP-seq, were deposited in the Genome Sequence Archive in National Genomics Data Center under accession number CRA015336, CRA015356, CRA015350 and CRA015361, respectively. Proteomics data from RNA interactome capture and mass spectrometry analysis of iPC cell lysates were deposited in iProX with the accession number IPX0002899001. The processed data of these experiments are provided in the Supplementary Information. Source data are provided with this paper.

References

1. Das, S. K., Lewis, B. A. & Levens, D. MYC: a complex problem. *Trends Cell Biol.* **33**, 235–246 (2023).
2. Bahrami, S. & Drablos, F. Gene regulation in the immediate-early response process. *Adv. Biol. Regul.* **62**, 37–49 (2016).
3. Decker, K. B., James, T. D., Stibitz, S. & Hinton, D. M. The Bordetella pertussis model of exquisite gene control by the global transcription factor BvgA. *Microbiology* **158**, 1665–1676 (2012).
4. Kayahara, M., Wang, X. & Tournier, C. Selective regulation of c-jun gene expression by mitogen-activated protein kinases via the 12-o-tetradecanoylphorbol-13-acetate- responsive element and myocyte enhancer factor 2 binding sites. *Mol. Cell Biol.* **25**, 3784–3792 (2005).
5. Ting, J. P. & Trowsdale, J. Genetic control of MHC class II expression. *Cell* **109**, S21–S33 (2002).
6. Chen, C. Y. & Shyu, A. B. Mechanisms of deadenylation-dependent decay. *Wiley Interdiscip. Rev. RNA* **2**, 167–183 (2011).
7. Herschman, H. R. Primary response genes induced by growth factors and tumor promoters. *Annu. Rev. Biochem* **60**, 281–319 (1991).

8. Lee, E. K. & Gorospe, M. Coding region: the neglected post-transcriptional code. *RNA Biol.* **8**, 44–48 (2011).
9. Grzybowska, E. A. & Wakula, M. Protein binding to Cis-Motifs in mRNAs coding sequence is common and regulates transcript stability and the rate of translation. *Cells* **10**, 2910 (2021).
10. Deenick, E. K. & Ma, C. S. The regulation and role of T follicular helper cells in immunity. *Immunology* **134**, 361–367 (2011).
11. Ochiai, K. et al. Transcriptional regulation of germinal center B and plasma cell fates by dynamical control of IRF4. *Immunity* **38**, 918–929 (2013).
12. Recaldin, T. & Fear, D. J. Transcription factors regulating B cell fate in the germinal centre. *Clin. Exp. Immunol.* **183**, 65–75 (2016).
13. Hu, Q. et al. Diverging regulation of Bach2 protein and RNA expression determine cell fate in early B cell response. *Cell Rep.* **40**, 111035 (2022).
14. Chang, X., Li, B. & Rao, A. RNA-binding protein hnRNPLL regulates mRNA splicing and stability during B-cell to plasma-cell differentiation. *Proc. Natl. Acad. Sci. USA* **112**, E1888–E1897 (2015).
15. Diaz-Munoz, M. D. et al. The RNA-binding protein HuR is essential for the B cell antibody response. *Nat. Immunol.* **16**, 415–425 (2015).
16. Bertossi, A. et al. Loss of Roquin induces early death and immune deregulation but not autoimmunity. *J. Exp. Med.* **208**, 1749–1756 (2011).
17. Xie, J. et al. The miR-17 approximately 92 miRNAs promote plasma cell differentiation by suppressing SOCS3-mediated NIK degradation. *Cell Rep.* **42**, 112968 (2023).
18. Castello, A. et al. System-wide identification of RNA-binding proteins by interactome capture. *Nat. Protoc.* **8**, 491–500 (2013).
19. Nojima, T. et al. In-vitro derived germinal centre B cells differentially generate memory B or plasma cells in vivo. *Nat. Commun.* **2**, 465 (2011).
20. Kwon, S. C. et al. The RNA-binding protein repertoire of embryonic stem cells. *Nat. Struct. Mol. Biol.* **20**, 1122–1130 (2013).
21. Boucas, J. et al. Label-free protein-RNA interactome analysis identifies Khsrp signaling downstream of the p38/Mk2 kinase complex as a critical modulator of cell cycle progression. *Plos One* **10**, e0125745 (2015).
22. Liepelt, A. et al. Identification of RNA-binding proteins in macrophages by interactome capture. *Mol. Cell Proteom.* **15**, 2699–2714 (2016).
23. Liao, Y. et al. The cardiomyocyte RNA-binding proteome: links to intermediary metabolism and heart disease. *Cell Rep.* **16**, 1456–1469 (2016).
24. Liao, J. Y. et al. EuRBPDB: a comprehensive resource for annotation, functional and oncological investigation of eukaryotic RNA binding proteins (RBPs). *Nucleic Acids Res.* **48**, D307–D313 (2020).
25. Fahl, S. P., Harris, B., Coffey, F. & Wiest, D. L. Rpl22 loss impairs the development of B lymphocytes by activating a p53-dependent checkpoint. *J. Immunol.* **194**, 200–209 (2015).
26. Wilmore, S. et al. Targeted inhibition of eIF4A suppresses B-cell receptor-induced translation and expression of MYC and MCL1 in chronic lymphocytic leukemia cells. *Cell Mol. Life Sci.* **78**, 6337–6349 (2021).
27. Monzon-Casanova, E. et al. The RNA-binding protein PTBP1 is necessary for B cell selection in germinal centers. *Nat. Immunol.* **19**, 267-+ (2018).
28. Su, Z. J. & Huang, D. Y. Alternative splicing of pre-mRNA in the control of immune activity. *Genes* **12**, 574 (2021).
29. Curdy, N. et al. Stress granules in the post-transcriptional regulation of immune cells. *Front. Cell Dev. Biol.* **8**, 611185 (2020).
30. Salerno, F. et al. An integrated proteome and transcriptome of B cell maturation defines poised activation states of transitional and mature B cells. *Nat. Commun.* **14**, 5116 (2023).
31. Joung, J. et al. Genome-scale CRISPR-Cas9 knockout and transcriptional activation screening. *Nat. Protoc.* **12**, 828–863 (2017).
32. Shaffer, A. L. et al. Blimp-1 orchestrates plasma cell differentiation by extinguishing the mature B cell gene expression program. *Immunity* **17**, 51–62 (2002).
33. Calado, D. P. et al. The cell-cycle regulator c-Myc is essential for the formation and maintenance of germinal centers. *Nat. Immunol.* **13**, 1092–1100 (2012).
34. Li, W. et al. MAGeCK enables robust identification of essential genes from genome-scale CRISPR/Cas9 knockout screens. *Genome Biol.* **15**, 554 (2014).
35. Hodgkin, P. D., Lee, J. H. & Lyons, A. B. B cell differentiation and isotype switching is related to division cycle number. *J. Exp. Med.* **184**, 277–281 (1996).
36. Henriksson, J. et al. Genome-wide CRISPR screens in T helper cells reveal pervasive crosstalk between activation and differentiation. *Cell* **176**, 882–896 e818 (2019).
37. Willis, S. N. et al. Transcription factor IRF4 regulates germinal center cell formation through a B cell-intrinsic mechanism. *J. Immunol.* **192**, 3200–3206 (2014).
38. Muto, A. et al. Bach2 represses plasma cell gene regulatory network in B cells to promote antibody class switch. *EMBO J.* **29**, 4048–4061 (2010).
39. Szklarczyk, D. et al. The STRING database in 2023: protein-protein association networks and functional enrichment analyses for any sequenced genome of interest. *Nucleic Acids Res.* **51**, D638–D646 (2023).
40. Turner, D. J. et al. A functional screen of RNA binding proteins identifies genes that promote or limit the accumulation of CD138+ plasma cells. *Elife* **11**, e72313 (2022).
41. Grenov, A., Hezroni, H., Lasman, L., Hanna, J. H. & Shulman, Z. YTHDF2 suppresses the plasmablast genetic program and promotes germinal center formation. *Cell Rep.* **39**, 110778 (2022).
42. Pelechano, V. & Alepuz, P. eIF5A facilitates translation termination globally and promotes the elongation of many non polyproline-specific tripeptide sequences. *Nucleic Acids Res.* **45**, 7326–7338 (2017).
43. Lee, A. S., Kranzusch, P. J. & Cate, J. H. eIF3 targets cell-proliferation messenger RNAs for translational activation or repression. *Nature* **522**, 111–114 (2015).
44. Liu, Y., Cui, J., Hoffman, A. R. & Hu, J. F. Eukaryotic translation initiation factor eIF4G2 opens novel paths for protein synthesis in development, apoptosis and cell differentiation. *Cell Prolif.* **56**, e13367 (2023).
45. Chang, T. C. et al. UNR, a new partner of poly(A)-binding protein, plays a key role in translationally coupled mRNA turnover mediated by the c-fos major coding-region determinant. *Genes Dev.* **18**, 2010–2023 (2004).
46. Reiner, J. E. Datta PK. TGF-beta-dependent and -independent roles of STRAP in cancer. *Front Biosci.* **16**, 105–115 (2011).
47. Carissimi, C. et al. Unrip is a component of SMN complexes active in snRNP assembly. *FEBS Lett.* **579**, 2348–2354 (2005).
48. Weidensdorfer, D. et al. Control of c-myc mRNA stability by IGF2BP1-associated cytoplasmic RNPs. *RNA* **15**, 104–115 (2009).
49. Murakawa, Y. et al. RC3H1 post-transcriptionally regulates A20 mRNA and modulates the activity of the IKK/NF-kappaB pathway. *Nat. Commun.* **6**, 7367 (2015).
50. Ito, K., Takahashi, A., Morita, M., Suzuki, T. & Yamamoto, T. The role of the CNOT1 subunit of the CCR4-NOT complex in mRNA deadenylation and cell viability. *Protein Cell* **2**, 755–763 (2011).
51. Gillen, S. L. et al. Differential regulation of mRNA fate by the human Ccr4-Not complex is driven by coding sequence composition and mRNA localization. *Genome Biol.* **22**, 284 (2021).
52. Uchiumi, T. et al. ERAL1 is associated with mitochondrial ribosome and elimination of ERAL1 leads to mitochondrial dysfunction and growth retardation. *Nucleic Acids Res.* **38**, 5554–5568 (2010).

53. Kim, E. et al. Mitochondrial aconitase suppresses immunity by modulating oxaloacetate and the mitochondrial unfolded protein response. *Nat. Commun.* **14**, 3716 (2023).
54. Sheppard, S. et al. Lactate dehydrogenase A-dependent aerobic glycolysis promotes natural killer cell anti-viral and anti-tumor function. *Cell Rep.* **35**, 109210 (2021).
55. Castello, A., Hentze, M. W. & Preiss, T. Metabolic enzymes enjoying new partnerships as RNA-binding proteins. *Trends Endocrinol. Metab.* **26**, 746–757 (2015).
56. Linxweiler, M., Schick, B. & Zimmermann, R. Let's talk about Secs: Sec61, Sec62 and Sec63 in signal transduction, oncology and personalized medicine. *Signal Transduct. Target Ther.* **2**, 17002 (2017).
57. Fischer, D. F. et al. Disease-specific accumulation of mutant ubiquitin as a marker for proteasomal dysfunction in the brain. *FASEB J.* **17**, 2014–2024 (2003).
58. Kamenska, A. et al. The DDX6-4E-T interaction mediates translational repression and P-body assembly. *Nucleic Acids Res.* **44**, 6318–6334 (2016).
59. Hunt, S. L., Hsuan, J. J., Totty, N. & Jackson, R. J. Unr, a cellular cytoplasmic RNA-binding protein with five cold-shock domains, is required for internal initiation of translation of human rhinovirus RNA. *Genes Dev.* **13**, 437–448 (1999).
60. Casola, S. et al. Tracking germinal center B cells expressing germline immunoglobulin gamma1 transcripts by conditional gene targeting. *Proc. Natl. Acad. Sci. USA* **103**, 7396–7401 (2006).
61. Van Nostrand, E. L. et al. Robust transcriptome-wide discovery of RNA-binding protein binding sites with enhanced CLIP (eCLIP). *Nat. Methods* **13**, 508–514 (2016).
62. Grosset, C. et al. A mechanism for translationally coupled mRNA turnover: interaction between the poly(A) tail and a c-fos RNA coding determinant via a protein complex. *Cell* **103**, 29–40 (2000).
63. Mao, Y. et al. m(6)A in mRNA coding regions promotes translation via the RNA helicase-containing YTHDC2. *Nat. Commun.* **10**, 5332 (2019).
64. Luo, W. et al. SREBP signaling is essential for effective B cell responses. *Nat. Immunol.* **24**, 337–348 (2023).
65. Carotta, S. et al. The transcription factors IRF8 and PU.1 negatively regulate plasma cell differentiation. *J. Exp. Med* **211**, 2169–2181 (2014).
66. Hodson, D. J. et al. Regulation of normal B-cell differentiation and malignant B-cell survival by OCT2. *Proc. Natl. Acad. Sci. USA* **113**, E2039–E2046 (2016).
67. Newman, R. & Tolar, P. Chronic calcium signaling in IgE(+) B cells limits plasma cell differentiation and survival. *Immunity* **54**, 2756–2771.e2710 (2021).
68. Miura, Y. et al. Bach2 promotes B cell receptor-induced proliferation of B lymphocytes and represses cyclin-dependent kinase inhibitors. *J. Immunol.* **200**, 2882–2893 (2018).
69. Ingolia, N. T., Ghaemmaghami, S., Newman, J. R. & Weissman, J. S. Genome-wide analysis in vivo of translation with nucleotide resolution using ribosome profiling. *Science* **324**, 218–223 (2009).
70. Chothani, S. et al. deltaTE: detection of translationally regulated genes by integrative analysis of Ribo-seq and RNA-seq data. *Curr. Protoc. Mol. Biol.* **129**, e108 (2019).
71. Moore, K. S. et al. Strap associates with Csde1 and affects expression of select Csde1-bound transcripts. *Plos One* **13**, e0201690 (2018).
72. Brown, E. C. & Jackson, R. J. All five cold-shock domains of Unr (upstream of N-ras) are required for stimulation of human rhinovirus RNA translation. *J. Gen. Virol.* **85**, 2279–2287 (2004).
73. Vukmirovic, M., Manojlovic, Z. & Stefanovic, B. Serine-threonine kinase receptor-associated protein (STRAP) regulates translation of type I collagen mRNAs. *Mol. Cell Biol.* **33**, 3893–3906 (2013).
74. Takeuchi, K. et al. Signaling pathways leading to transcription and translation cooperatively regulate the transient increase in expression of c-Fos protein. *J. Biol. Chem.* **276**, 26077–26083 (2001).
75. Lemm, I. & Ross, J. Regulation of c-myc mRNA decay by translational pausing in a coding region instability determinant. *Mol. Cell Biol.* **22**, 3959–3969 (2002).
76. Yeh, E. et al. A signalling pathway controlling c-Myc degradation that impacts oncogenic transformation of human cells. *Nat. Cell Biol.* **6**, 308–318 (2004).
77. Guo, A. X., Cui, J. J., Wang, L. Y. & Yin, J. Y. The role of CSDE1 in translational reprogramming and human diseases. *Cell Commun. Signal* **18**, 14 (2020).
78. Corley, M., Burns, M. C. & Yeo, G. W. How RNA-binding proteins interact with RNA: molecules and mechanisms. *Mol. Cell* **78**, 9–29 (2020).
79. Behrens, G. & Heissmeyer, V. Cooperation of RNA-binding proteins —a focus on roquin function in T cells. *Front Immunol.* **13**, 839762 (2022).
80. Jin, L. et al. STRAP regulates alternative splicing fidelity during lineage commitment of mouse embryonic stem cells. *Nat. Commun.* **11**, 5941 (2020).
81. Balcerak, A., Trebinska-Stryjewska, A., Konopinski, R., Wakula, M. & Grzybowska, E. A. RNA–protein interactions: disorder, moonlighting and junk contribute to eukaryotic complexity. *Open Biol.* **9**, 190096 (2019).
82. Haniuda, K., Nojima, T. & Kitamura, D. In vitro-induced germinal center B cell culture system. *Methods Mol. Biol.* **1623**, 125–133 (2017).
83. Tyanova, S. et al. The Perseus computational platform for comprehensive analysis of (prote)omics data. *Nat. Methods* **13**, 731–740 (2016).
84. Pertea, M., Kim, D., Pertea, G. M., Leek, J. T. & Salzberg, S. L. Transcript-level expression analysis of RNA-seq experiments with HISAT, StringTie and Ballgown. *Nat. Protoc.* **11**, 1650–1667 (2016).
85. Love, M. I., Huber, W. & Anders, S. Moderated estimation of fold change and dispersion for RNA-seq data with DESeq2. *Genome Biol.* **15**, 550 (2014).
86. Zhou, Y. et al. Metascape provides a biologist-oriented resource for the analysis of systems-level datasets. *Nat. Commun.* **10**, 1523 (2019).
87. Van Nostrand, E. L. et al. Principles of RNA processing from analysis of enhanced CLIP maps for 150 RNA binding proteins. *Genome Biol.* **21**, 90 (2020).
88. Smith, T., Heger, A. & Sudbery, I. UMI-tools: modeling sequencing errors in Unique Molecular Identifiers to improve quantification accuracy. *Genome Res.* **27**, 491–499 (2017).
89. Liu, Q. & Gregory, R. I. RNAmod: an integrated system for the annotation of mRNA modifications. *Nucleic Acids Res.* **47**, W548–W555 (2019).
90. Ingolia, N. T., Brar, G. A., Rouskin, S., McGeachy, A. M. & Weissman, J. S. The ribosome profiling strategy for monitoring translation in vivo by deep sequencing of ribosome-protected mRNA fragments. *Nat. Protoc.* **7**, 1534–1550 (2012).
91. Morlan, J. D., Qu, K. & Sinicropi, D. V. Selective depletion of rRNA enables whole transcriptome profiling of archival fixed tissue. *Plos One* **7**, e42882 (2012).
92. Xiao, Z. et al. De novo annotation and characterization of the translatome with ribosome profiling data. *Nucleic Acids Res* **46**, e61 (2018).
93. Dobin, A. et al. STAR: ultrafast universal RNA-seq aligner. *Bioinformatics* **29**, 15–21 (2013).
94. Li, F., Xing, X., Xiao, Z., Xu, G. & Yang, X. RiboMiner: a toolset for mining multi-dimensional features of the translatome with ribosome profiling data. *BMC Bioinforma.* **21**, 340 (2020).

95. Jin, H. Y. et al. Differential sensitivity of target genes to translational repression by miR-17~92. *PLoS Genet.* **13**, e1006623 (2017).
96. Chen, C. Y., Ezzeddine, N. & Shyu, A. B. Messenger RNA half-life measurements in mammalian cells. *Methods Enzymol.* **448**, 335–357 (2008).

Acknowledgements

We thank Jianfeng Wu and Kang Yang for assistance with mouse breeding and B cell experiments, Xin Zeng (Sanofi Institute for Biomedical Research) and Zecheng Zuo lab for quantitative mass spectrometry, Tuan Qi (Xing Chang lab) for assistance with RBP interactome capture experiments, Ziwei Chen (Dan Du lab) for establishing mouse models, Zhengtao Xiao (Xi'an Jiaotong University) for advice on Ribo-seq data analysis, Xu Zhang (Suzhou Institute of Systems Medicine) for advice on data processing, Jiahuai Han lab for providing cell lines and plasmids, Alex Shishkin and Kylie Shen at Eclipse BioInnovations for their kind help with eCLIP experiments and data analysis. This study is supported by the National Key R&D Program of China (2022YFA1304000 to D.D.), the National Natural Science Foundation of China (82372788 to D.D., 81961138008 to C. X., 31770950 and 32070877 to W.-H.L., 32025016 & 82450102 to X.C.), "Pioneer" and "Leading goose" R&D program of Zhejiang (2022SDXHDX0002 to X.C.), the Shanghai Municipal Science and Technology Major Project (Y.Z), the Shanghai Basic Research Pioneer Project (Y.Z), the Shanghai Key Laboratory of Aging Studies (19DZ2260400 to Y.Z) and Sanofi Institute for Biomedical Research (SIBR).

Author contributions

C.X., P.C., X.C., and D.D. conceptualized and designed the project. P.C., L.L., X.L. performed most of the experiments. K.L. performed RNA imaging and eCLIP experiments. J.W. assisted in mouse strain acquisition and breeding. J.Q. and Y.Z. performed MS experiments and data analysis for mRNA-interactome capture. X.Z., L.Y., and N.Y. performed quantitative MS analysis of total cell lysates. Y.L. and H.S. performed some of polysome profiling and plasmid construction experiments. P.C. and K.L. performed most of the bioinformatic analyses. P.C., K.L., L.L., X.L., Z.W., X.C., D.D., and C.X. contributed to data interpretation and discussions. Y.H. managed experimental reagents and supplies. P.C., D.D., and C.X. interpreted the results and wrote the manuscript with contributions from all authors. W.-H.L., D.D., and C.X supervised the project.

Competing interests

The authors declare no competing interests.

Additional information

Supplementary information The online version contains supplementary material available at https://doi.org/10.1038/s41467-025-58212-8.

Correspondence and requests for materials should be addressed to Wen-Hsien Liu, Yaoyang Zhang, Xing Chang, Dan Du or Changchun Xiao.

Peer review information *Nature Communications* thanks the anonymous reviewer(s) for their contribution to the peer review of this work. A peer review file is available.